minerals

MDPI

Article

Age of Gold Mineralizations of Dongping and Xiaoyingpan Gold Deposits in North China Craton: Constraints from the Zircon U–Pb Dating and Fission-Track Analysis

Yunlei Feng [1,2], Hao Wei [1,*], Dong Li [1,2] and Wenbiao Du [1,2]

1 Hebei Key Laboratory of Strategic Critical Mineral Resources, Hebei GEO University, Shijiazhuang 050031, China; yunlei_feng@126.com (Y.F.); lidongcugb@126.com (D.L.); dwenbiao0327@163.com (W.D.)
2 College of Earth Sciences, Hebei GEO University, Shijiazhuang 050031, China
* Correspondence: ronghaiwei@163.com

Abstract: Northwest Hebei province is one of the gold-producing areas in China. Based on a geochronological analysis of the Zhangjiakou-Xuanhua area, zircon U–Pb with an age of 2487–142 Ma and zircon fission-track (ZFT) with a cooling age of 155–66 Ma were obtained. Zircon U–Pb dating of the Xiaoyingpan deposit revealed two ages of 2487 ± 92 Ma and 1745 ± 89 Ma, representing the Archaean and Early Proterozoic metamorphism of the Sanggan Group. The ZFT cooling age of 155 ± 10 Ma represents the deposit's lower limit metallogenic age. The Shuiquangou (SQG) alkaline complex emplaced at 388.9 ± 3.0 Ma and experienced magmatic activities until the Late Devonian (ca 377 Ma), considering the response to the collision between the Siberian plate and the North China Craton. The emplacement age of Shangshuiquan (SSQ) granite is 142.3 ± 1.1 Ma and is coeval with the thinning of the North China Craton during the Late Jurassic–Early Cretaceous. The intrusion of SSQ might partially reheat the SQG complex, resulting in the Yanshanian gold mineralization in Dongping. The SQG complex and SSQ granite underwent a relatively consistent rapid cooling process in the Cretaceous based on the ZFT ages.

Keywords: Dongping gold deposit; Xiaoyingpan gold deposit; Shuiquangou alkaline complex; Shangshuiquan granite; Zircon U–Pb dating; Zircon fission-track thermochronology

Citation: Feng, Y.; Wei, H.; Li, D.; Du, W. Age of Gold Mineralizations of Dongping and Xiaoyingpan Gold Deposits in North China Craton: Constraints from the Zircon U–Pb Dating and Fission-Track Analysis. *Minerals* **2022**, *12*, 831. https://doi.org/10.3390/min12070831

Academic Editor: Simon Paul Johnson

Received: 19 May 2022
Accepted: 27 June 2022
Published: 29 June 2022

1. Introduction

More than one-fifth of large-super large Cu-Au (Mo) deposits globally are related to alkaline magmas [1] and have attracted more and more attention in the past few decades. The northwestern Hebei gold mineralization area is an essential part of the gold metallogenic belt in the North China Craton (NCC). Since the discovery of the Xiaoyingpan gold deposit in 1965, more than 100 gold deposits in different scales have been detected in this area, including two large gold deposits (the Xiaoyingpan gold deposit and the Dongping gold deposit, respectively). The Dongping Gold Deposit is the most typical world-class gold deposit in an alkaline complex in the NCC [2]. The Xiaoyingpan gold deposit, which is only 16 km away from Dongping, is hosted in the outer contact zone of the alkaline complex and is also one of the large gold deposits attracting focus in northwest Hebei province China.

However, there are still many disputes on the genesis of gold deposits in this area. Although the Dongping gold deposit is hosted in the Shuiquangou (SQG) alkaline complex, which is invaded by the surrounding multi-stage granitic intrusions, there are some different views on whether mineralization is entirely affected by synchronous magmatism or hydrothermal activities. Previous studies [3–5] indicated that there are non-negligible time gaps between the surrounding plutons' diagenesis and gold mineralization. Therefore, the Dongping gold deposit was suggested to have no genetic relationship with the surrounding SQG alkaline complex and Yanshanian Shangshuiquan granite. The oldest age of the intrusions in the study area obtained is about 1719 Ma. At the same time, the youngest mineralization time is approximately 120 Ma, indicating frequent magmatism, hydrothermal activities, and tectono-thermal events in the region. However, studies on the source of ore-forming materials, fluid composition, and geochemistry of trace elements [6–11] revealed the genetic relationship between the Dongping gold deposit and the surrounding magmatism. Furthermore, the relationship between the ore-forming process and the surrounding magmatism of the Xiaoyingpan gold deposit outside the SQG complex is also unclear.

If mineralization and diagenesis are related, they should be consistent in time and thermal background. Previous studies on the chronology of plutons and ore deposits in this area have involved various dating methods, including the high-temperature chronometers (e.g., zircon U/Pb, hornblende or biotite $^{40}Ar/^{39}Ar$) [12–14] and intermediate-temperature thermochronometers (e.g., K-feldspar or sericite $^{40}Ar/^{39}Ar$, and K-feldspar K-Ar) [13,15–20]. These ages range from 389 Ma to 103 Ma. Some of these ages can represent emplacement ages, while others are suitable for cooling ages only because the closure temperature of different dating methods varies. Thus, the interpretation of these ages will directly determine the reconstruction of the magmatic-thermal history of the region. The metallogenic temperatures of Dongping and Xiaoyingpan deposits are approximately 250–380 °C [21,22] and 265–348 °C [23,24], respectively, based on the analyses of fluid inclusions in gold-bearing quartz veins by the homogeneous method. Therefore, low-temperature thermochronology, especially zircon fission-track dating, is suitable for limiting the end time of gold mineralization. However, no low temperature thermochronology data for the study area can be obtained, which poses a significant challenge in rebuilding the thermal history and defining the thermal reset caused by magma emplacement. Therefore, from the perspective of time and temperature consistency, this paper will combine zircon U–Pb dating and zircon fission-track (ZFT) dating to analyze the chronology and thermal history of the intrusions and deposits in this area to unveil the relationship between the multi-stage magmatism and the gold deposits.

2. Regional and District Geological Setting

2.1. Regional Geological Setting

The Zhangjiakou-Xuanhua area is tectonically located on the western end of the Yanshan orogen [12] in the middle part of the northern margin of the NCC. The Shangyi-Chicheng-Damiao (SCD) E-W trending deep-rooted fault, also regarded as the demarcation between the Inner Mongolia axis and NCC [25], was formed in the Mesoproterozoic and continuously reactivated in the Neoproterozoic, Paleozoic, and Mesozoic [26,27]. The minimum distance between the SCD fault and the gold deposits hosted in the SQG alkaline complex, such as Dongping, Zhongshangou, and Hougou, is only 10 km (Figure 1).

Archean and Early Proterozoic metamorphic rocks are widely distributed in the study area, including Sanggan Group, Chongli Group, and Hongqiyingzi Group. The SCD fault separates the Sanggan Group, a set of amphibolite-granulite metamorphic rock series, to the south and the medium-grade metamorphic Hongqiyingzi Group to the north. The chronological results of these three strata are relatively broad. The Sanggan Group is formed in 3849–1148 Ma, while the Chongli Group in 3068–1148 Ma. The Hongqiyingzi Group is younger (2657–1757 Ma). The Paleoproterozoic Hongqiyingzi Group outcrops north of the SCD deep fault and appears in the EW-trending belt in the Liujianfang-Shangyouyang area. This stratum consists of volcanic-sedimentary formations. The lower part is mainly pyroclastic rocks mixed with intermediate-basic volcanic rocks. The upper part gradually evolves into continental pyroclastic rocks mixed with intermediate and intermediate-acid volcanic rocks. The top part is sand, mud, and carbonate deposits formed in the shallow sea depositional environment. Mesoproterozoic marine sedimentary occur sparsely in the southeastern corner of the study area. However, the volcanic lava and pyroclastic rocks of the Mesozoic Zhangjiakou Formation overlay the Archean strata in the central part of this area.

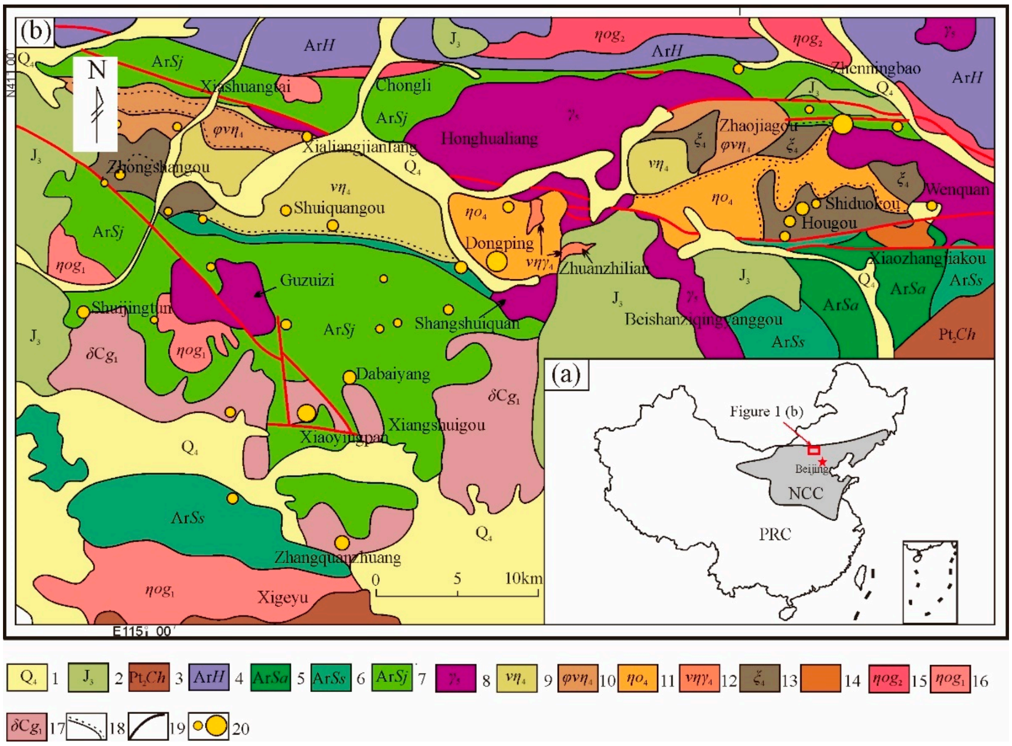

Figure 1. Simplified map of the geology of Northern Hebei Province showing the locations of gold deposits (modified after Wang et al. [7] and Zhen et al. [28]) (**a**,**b**). 1—Quaternary; 2—Yanshanian intermediate-acidic volcaniclastic rocks; 3—Changcheng System; 4—Hongqiyingzi Group; 5—Aijiagou Formation, Sanggan Group; 6—Shuidizhuang Formation, Sanggan Group; 7—Jianhegou Formation, Sanggan Group; 8—granite; 9—hornblende monzonite; 10—pyroxene amphibolite; 11—quartz monzonite; 12—hornblende monzogranite; 13—syenite; 14—pyroxenite; 15—Proterozoic granitic; 16—Archean granitic gneiss; 17—Archean metamorphic tonalite; 18—migmatite belt; 19—faults; 20—gold deposits; PRC-People's Republic of China; NCC-North China Craton.

The widespread multi-stage intrusions mainly occur on the south side of the SCD fault in this area. The granitic gneiss in the metamorphic Sanggan Group is the earliest intrusion found in this area. The Paleoproterozoic intrusions mainly include the Wenquan porphyritic granites and ultrabasics along Shizuizi-Zhenningpu. The Xiaozhangjiakou ultrabasic intrusion sparsely occurs in Jinjiazhuang-Xiaozhangjiakou-Yujiagou, and it is the only Mesoproterozoic intrusive rock in the study area. The SQG alkaline syenite and Guzuizi porphyritic granite are the typical Varisian and Indosinian intrusions in this region, respectively. In addition, the widespread Yanshanian magmatism in the region led to the formation of the Beiljiazi biotite monzogranite, Honghuoliang biotite granite, and the Shangshuiquan (SSQ) potassic feldspar granite.

The SQG alkaline syenite complex is mainly composed of monzonite and syenite, and the boundary between them is not apparent. First, the complex intruded into the Archean metamorphic rocks (Figure 2a) and outcrops along the south of the SCD deep-root fault as a narrow belt of 55 km in length and 5–8 km in width. Then, the Honghualiang granite, SSQ granite (Figure 2b), and Wenquan granite intruded north, south, and east of the SQG complex, followed by the eruption of the Early Cretaceous Zhangjiakou Formation (Figure 2c,d) covered the western and central parts of the intrusions.

The Guzuizi porphyritic granites intruded into the Jianguohe Formation of Sanggan Group and were dated to have formed during the Yanshanian (the whole-rock Rb-Sr isochronous age of (184 ± 24) Ma [29]. However, the zircon U–Pb age of 236 Ma [30] demonstrates the Triassic emplacement of the intrusion.

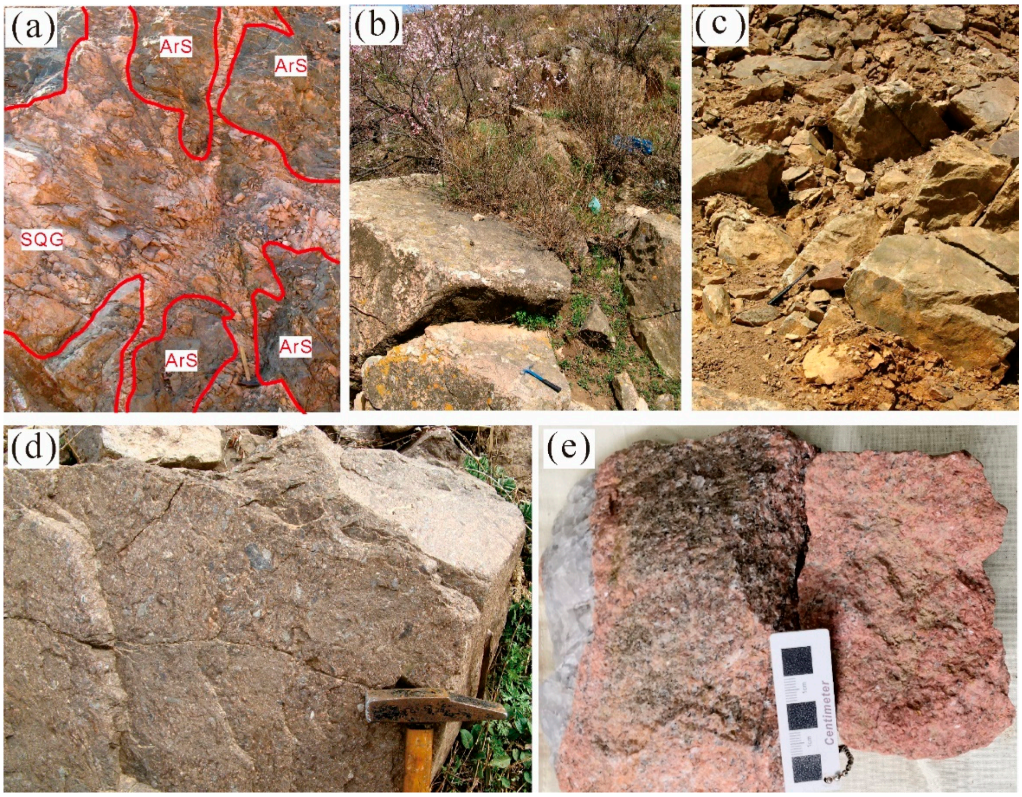

Figure 2. Photographs of occurrences and samples from the Zhangjiakou-Xuanhua area. (**a**) plagiogneiss of Sanggan Group crosscut by later syenite veins; (**b**) outcrop of the Shangshuiquan granite; (**c**) outcrop of the Shuiquangou complex; (**d**) outcrop of the Zhangjiakou Formation; (**e**) potassic host rock and quartz veins. Abbreviations: ArS = Archean Sanggan Group, SQG = Shuiquangou alkaline complex.

The SSQ K-feldspar granite occurs in Yaoziwan-Shangshuiquan with an irregular oval shape and an outcropping area of about 8 km^2 to the southeast of the Dongping gold deposit. The SSQ intrusion comprises medium-grained biotite potassic feldspar granite with crystal caves and quartz clusters.

In recent years, geochronological dating [4,12,31,32] has indicated that the SQG alkaline complex's formation age should be around 400 Ma. However, unlike the Hercynian diagenesis, many studies have pointed out that the SQG complex may have formed in the later geological age [15–17].

For the Yanshanian granites in the region, Miao et al. [30] determined that the emplacement age of SSQ potassic feldspar granite is 142.5 $\pm$ 1.3 Ma based on the SHRIMP zircon U–Pb dating. Similarly, Jiang et al. [33] obtained 142.9 $\pm$ 0.8 Ma using SHRIMP zircon U–Pb dating. The Zhuanzhilian (ZZL) porphyritic granite, occurring within the SQG complex, was formed at 143–139.5 Ma [33–35].

2.2. Ore Deposit Geology

The Dongping gold deposit is located in the central part of SQG syenite near the village of Dongping (Figure 3) [12], south of the SCD deep-root deep fault. In the southern contact zone, ore bodies occur between the syenite and the Archean metamorphic rocks. Faults in the Dongping gold mine area are well-developed. The NW-trending Yangmuwa-Majangzi-Jinjiazhuang fault and the Zhongshagou-Honghuabi-Shangshuiquan fault are the two most essential secondary faults that control the north and south boundary of the Dongping gold mine, respectively [36]. In addition to the SQG alkaline complex, other intrusions still outcrop around the ore bodies, such as the SSQ potassic feldspar granite, Honghuoliang alkali feldspar granite, ZZL porphyritic granite (Figure 4a), and intermediate-acid dikes.

More than 70 gold-bearing veins (Figure 4b) in the mining area vary in size and occurrence. Tectonic shear zones often occur between ore veins and surrounding rock, resulting in the fragmentation and elongation of mineral grains (Figure 4c,d). The veins can be divided into nine NNE-NE trending mineralization belts based on the orebody characteristics. The ore types of Dongping gold deposits can be divided into quartz vein type and potassium-silicide alteration type. There is no extinct boundary between these two ore types, and potassium-silicide alteration can be seen near quartz veins in the middle segment of the main orebody. The ores mainly consist of sulfides, such as pyrite, galena, sphalerite, and chalcopyrite, and lesser amounts of oxides, such as hematite and magnetite.

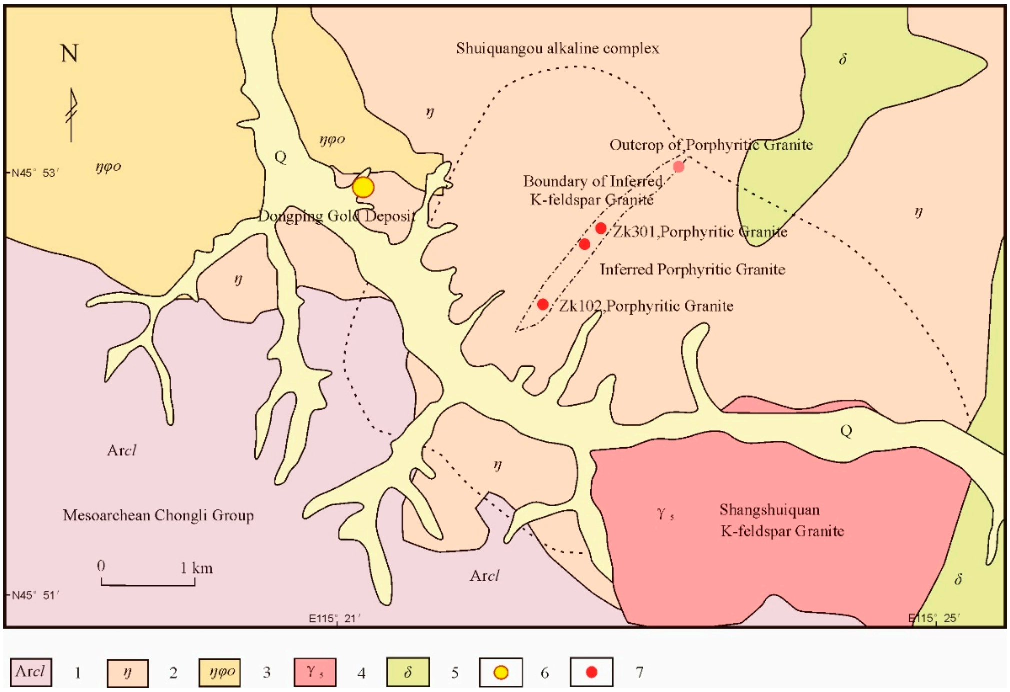

Figure 3. Sketch map of the Dongping gold deposit (after 1:10,000 geological map surveyed by Geological Exploration Report of Dongping Deposit, Chongli Zijin Mining Co., Ltd., Zhangjiakou, China, 2012). 1—Archean Chongli group metamorphic rocks; 2—Shuiquangou alkaline complex; 3—hornblende monzonite; 4—Shangshuiquan K-feldspar granite; 5—diorite; 6—gold deposit; 7—drill.

The Xiaoyingpan gold deposit is located 8-20 km south of the SCD fault, covering approximately 9 km^2. The Proterozoic Sanggan Group constitutes the ancient crystalline basement of the Xiaoyingpan deposit (Figure 5). No intrusion occurs in the mining area, but the dikes are well-developed. Nevertheless, the Guzuizi granite intrudes into the north of the mining area, and the distance between them is just about 4 km. Two NNW trending faults mainly control the ore bodies of the Xiaoyingpan gold deposit. As a result, more than 30 gold-bearing quartz veins occur sporadically in a lenticular shape, forming the gold belt in Xiaoyingpan. The alteration in wall rocks includes potassic feldspar (Figure 2e), silicification, sericitization, pyritization, and carbonation. The alteration zonation is not apparent. In addition, the width of the alteration zone is associated with the thickness of the quartz vein. Hence, the thick alteration zone in the footwall of the quartz vein resulted in the local enrichment of Au, forming the altered-rock type of gold orebodies. Ores are massive, disseminated, and net-veined, consisting of pyrite, chalcopyrite, galena, and sphalerite (Figure 4e).

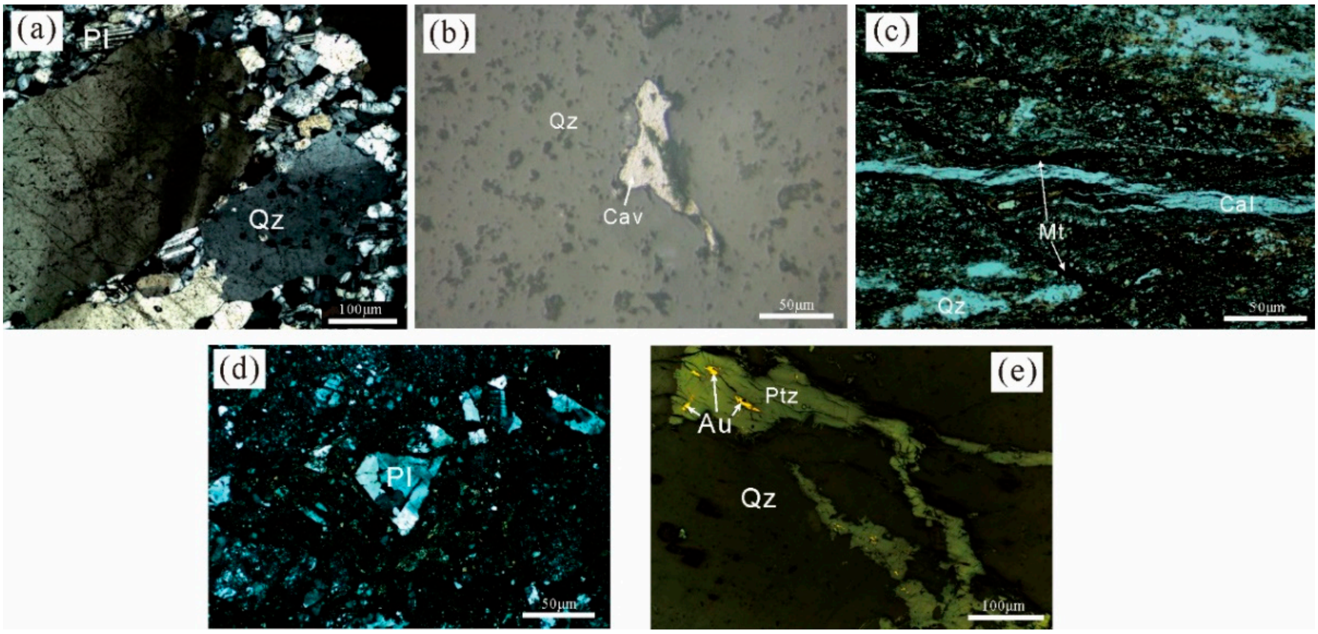

Figure 4. Photomicrographs and reflected-light photomicrographs of samples from the Zhangjiakou-Xuanhua area. (**a**) lenticular quartz porphyry in ZZL porphyritic granites containing plagioclase grains; (**b**) calaverite hosted in quartz veins in Dongping deposit; (**c**,**d**) fragmentation and elongation of mineral grains in tectonic shear zones in Dongping deposit; (**e**) native gold grain included in petzite hosted by quartz vein in Xiaoyingpan deposit. Abbreviations: Cal = calcite, Cav = calaverite, Mt = magnetite, Pl = plagioclase, Ptz = petzite, Qz = quartz.

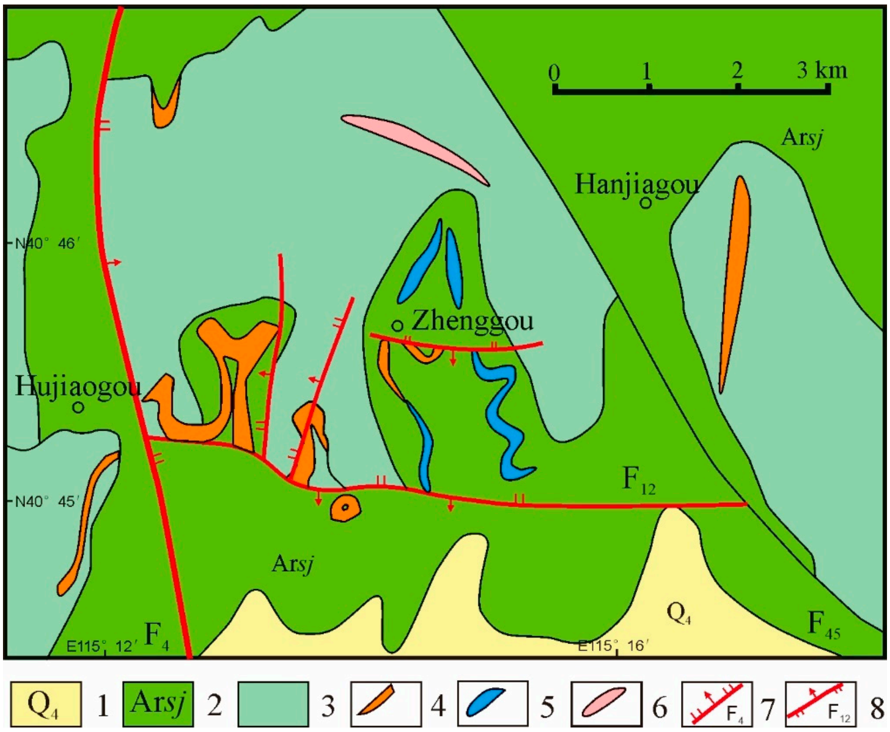

Figure 5. Sketch map of the Xiaoyingpan gold deposit (modified after Jiang and Nie [24], Song and Wang [37]). 1—Quaternary; 2—Jianhegou Formation, Sanggan Group; 3—Huajiaying Formation, Sangan Group; 4—gold-bearing quartz veins; 5—altered belts; 6—altered-rock type of gold orebodies; 7—normal faults; 8—reverse faults.

3. Materials and Methods

To better understand the study area's regional geology and cooling history, samples were collected across the mineralized area and host rocks for zircon U–Pb and zircon fission-track analysis. Zircon concentrates were extracted from crushed rock samples using standard magnetic and heavy-liquid separation techniques at the Hebei Institute of Geological and Mineral Survey (Langfang, China). Cathodoluminescence (CL) images of zircon grains were obtained at Beijing GeoAnalysis Co., Ltd. (Beijing, China) to select distinct zircon domains by unveiling internal structures.

3.1. U–Pb Dating

Dating of samples was performed by the instrument for zircon U–Pb dating and trace element analysis at Hebei Key Laboratory of Strategic Critical Mineral Resource of Hebei Geo University, which is equipped with a quadrupole ICP-MS (iCAP RQ) and 193 nm ArF Excimer laser (RESOlution-LR) with a Laurin Technic S155 sample-chamber and GeoStar µGISTM software. Laser ablation was operated at a constant energy density of 3 J/cm^2 with a spot diameter of 19µm and a repetition rate of 8 Hz. Each analysis includes 10 seconds blank, a 40 s sample ablation, and a 20 s sample chamber flushing after the ablation, and the ablated material was transported to the ICP-MS by the high-purity helium gas stream [38]. Two zircon 91,500 standards, one zircon GJ-1, and one NIST SRM610 were measured at each of the five sample sites to supervise the deviation of age calculation. The NIST SRM 610 is used as an external standard and Si is as the internal standard to calibrate the trace element concentration. Isotope ratio data processing was calculated by ICPMSDataCal [39] and Isoplot (version 3.0 [40]) programs.

3.2. Zircon Fission Track Analysis

Zircon grains were mounted on FEP Teflon wafers and then polished with diamond paste. The spontaneous tracks were revealed by etching in a eutectic (1:1) mixture of KOH and NaOH at 220 °C for about 22 h.

The uranium-poor muscovite flakes were placed as the external detector adjacent to the etched sample mounts, which were then irradiated with thermal neutrons in the well thermalized (Cd value for Au > 100) 492 Swim-pool hot neutron nuclear reactor based at the Beijing Institute of High Energy Physics, Chinese Academy of Sciences. The external detectors were detached from the mineral mounts and etched in 40% HF for 20 min at 25 °C to reveal the induced fission tracks after irradiation. Both spontaneous and induced fission tracks populations were counted under the microscope with a 100× dry objective and an overall magnification of 1500 to calculate the track densities of external detectors and sample mounts, respectively. Neutron fluence was monitored with the CN2 and CN5 uranium dosimeter glasses [41]. Only crystals with prismatic sections parallel to the c-crystallographic axes were accepted for analysis as these crystals have the lowest bulk etch rate [42].

The Zeta calibration approach [43,44] was used to calculate the fission-track central ages [45]. A > 5% probability of the chi-square test [46] demonstrates that all age grains tested belong to a single population. Errors were calculated following Green [47].

4. Results

4.1. The Shuiquangou Alkaline Complex

A total of three samples were collected from the SQG alkaline complex and selected for subsequent geochronology test of zircon LA-ICP-MS U–Pb and fission track. Sample F-3-2 and F-4 are fresh and alternated K-feldspar pegmatite were collected within the pegmatite dike in the ZZL district, respectively. Sample D-9 is altered cataclasite next to the underground gold-bearing quartz veins in the Dongping deposit. Sufficient zircon grains were separated from these three samples despite the diversity in morphology.

Zircon grains from F-3-2, F-4, and D-9 are generally broken with localized magmatic oscillatory zoning in CL images, suggesting a magmatic origin (Figure 6). The zircon grains in D-9 are about 30–80μm in size, while that in F-3-2 and F-4 are 80–200 μm and 80–120 μm, respectively. Most zircon grains in these three samples show well-developed growth zoning, whereas some grains show that regular growth zoning is interrupted by textural discontinuities, along which the original zoning is resorbed and succeeded by the deposition of new growth-zoned zircon. These textures suggest that it may have been formed by the very slow and complex crystallization of a magma body with prolonged residence time in the lower crust [48]. The REE concentrations of zircon grains and fragments in F-4 vary between 331 and 4989 ppm, while F-3-2 and D-9 are relatively low at 20–693 ppm and 13–177 ppm, respectively (Table 1). They all show normalized patterns characterized by a steeply rising slope from the LREE to the HREE with positive Ce anomalies (with Ce/Ce* values mostly higher than 20) (Figure 7), indicating typical characteristics of magmatic zircon [49].

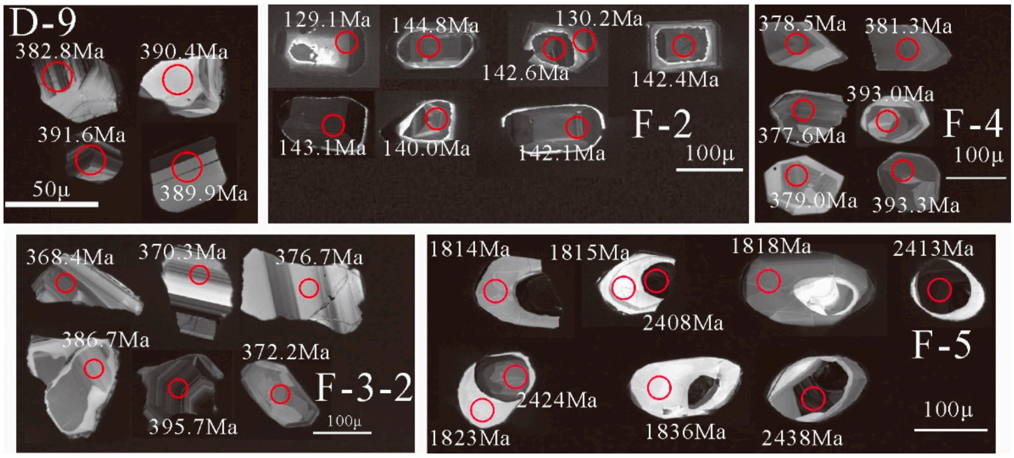

Figure 6. Cathodoluminescence images of zircon from samples in the Zhangjiakou-Xuanhua area. Red circles—spots of U-Pb analysis on zircon.

The thorium and uranium content of the zircon grains from F-3-2 varies within a relatively wide range, with the Th/U ratios ranging from 0.20 to 0.86, typical for magmatic zircons. A total of 22 analyses of LA-ICPMS U–Pb were carried out upon 18 zircon grains and fragments from F-3-2, which yielded $^{206}Pb/^{238}U$ age with a weighted average of 381.2 ± 3.8 Ma with MSWD = 3.3 (Table 2, Figure 8). A similar age was obtained from the sample of alternated K-feldspar pegmatite (F-4), which yielded 381.0 ± 3.9 Ma (MSWD = 2.6). This probably demonstrates that all zircons show a magmatic age for the SQG alkaline complex with a value of 376-393 Ma. The slow and complex crystallization history results in these samples' wide age ranges. A total of 11 LA-ICPMS U–Pb measurements of zircon grains in D-9 yielded slightly older ages with an average of 388.9 ± 3.0 Ma, MSWD = 0.72 with Th/U ratio of 0.09–0.98. This indicates the forming ages of the magmatic zircon grains captured into the altered cataclasite by later tectonic movements. This age alone, with the ages of F-3-2 and F-4, is close to the forming age of the SQG complex and may indicate the emplacement age of the alkaline complex.

Table 1. REE composition of zircons from samples in Zhangjiakou-Xuanhua area (ppm).

	La	Ce	Pr	Nd	Sm	Eu	Gd	Tb	Dy	Ho	Er	Tm	Yb	Lu	Ce/Ce* [1]	Eu/Eu* [2]	REE
D-9-07	0.00	30.10	0.30	2.26	2.14	0.89	5.30	1.29	12.67	4.04	16.80	3.81	40.80	8.13	31.15	0.77	128.53
D-9-08	0.00	10.33	0.11	0.78	0.39	0.18	0.60	0.16	1.73	0.59	2.83	0.71	8.67	1.94	29.15	1.13	29.04
D-9-10	0.00	24.96	0.67	4.09	1.61	0.72	2.75	0.56	5.65	1.74	7.12	1.68	18.93	4.06	11.57	1.04	74.54
D-9-11	0.00	13.04	0.21	1.40	0.68	0.31	1.16	0.22	2.32	0.79	3.56	0.95	10.50	2.54	19.28	1.06	37.70
D-9-13	0.00	6.98	0.02	0.06	0.05	0.06	0.19	0.03	0.46	0.18	0.90	0.21	3.08	0.68	108.35	1.65	12.89
D-9-16	0.00	12.39	0.16	0.95	0.85	0.51	2.47	0.59	5.11	1.57	5.90	1.46	15.25	3.12	24.04	1.00	50.34
D-9-18	0.12	130.03	8.05	23.76	1.72	2.07	1.49	0.22	1.83	0.43	1.58	0.43	4.20	0.87	4.98	3.86	176.81
D-9-21	0.00	23.09	0.30	2.12	1.49	0.70	4.26	0.90	8.95	2.61	10.66	2.55	25.75	5.27	23.89	0.79	88.66
D-9-23	0.01	103.25	1.29	5.04	1.33	1.10	3.28	0.79	7.09	1.72	5.80	1.14	10.94	1.73	24.77	1.54	144.53
D-9-31	0.00	37.52	0.45	2.54	1.18	0.41	1.60	0.35	3.26	0.91	3.95	1.07	13.61	3.29	25.89	0.91	70.15
D-9-32	0.01	23.28	0.24	1.69	1.85	0.88	4.24	1.12	10.64	3.22	13.19	3.41	37.99	8.13	29.62	0.93	109.88
F-2-5	0.10	32.43	1.21	7.28	15.74	0.13	83.77	33.75	441.31	161.49	679.23	150.57	1309.14	206.30	8.05	0.01	3122.45
F-2-8	0.02	47.79	0.41	4.11	13.99	0.18	79.58	31.32	395.88	143.09	592.78	130.80	1123.98	178.99	35.49	0.01	2742.90
F-2-12	0.04	32.66	0.59	4.44	11.68	0.07	70.21	28.33	366.93	132.49	545.44	117.72	1008.90	159.15	16.73	0.01	2478.65
F-2-20	2.33	95.74	29.16	57.77	28.68	0.12	89.50	33.41	407.73	145.61	591.57	128.20	1083.66	170.94	0.99	0.01	2864.41
F-2-21	0.34	100.24	4.49	20.48	34.35	0.41	150.29	53.29	637.52	220.14	876.68	188.08	1590.65	249.55	6.73	0.01	4126.52
F-2-22	0.04	50.89	1.02	6.89	17.87	0.17	98.52	39.83	501.27	181.17	751.36	164.14	1429.19	225.55	15.25	0.01	3467.92
F-2-27	0.07	56.93	1.00	6.07	16.02	0.23	88.79	34.85	441.05	158.69	653.58	143.30	1231.14	196.96	17.19	0.01	3028.69
F-2-32	0.01	64.22	0.48	4.79	16.34	0.20	93.56	34.86	430.70	151.67	604.36	131.42	1111.73	176.98	41.19	0.01	2821.32
F-2-34	0.00	58.74	0.43	4.77	10.76	0.28	52.43	19.03	231.39	81.54	332.38	70.74	613.27	98.08	42.41	0.03	1573.85
F-2-39	0.01	59.64	0.60	6.44	14.22	0.41	65.76	23.55	282.61	99.57	399.52	85.96	756.88	119.85	30.65	0.03	1915.02
F-2-45	0.01	40.74	0.62	6.53	18.59	0.32	92.22	35.18	432.26	154.87	626.39	137.34	1180.97	187.78	20.27	0.02	2913.83
F-3-2-4	0.00	11.38	0.03	0.43	0.40	0.25	0.85	0.32	3.41	1.29	6.22	1.89	23.66	5.52	117.77	1.28	55.65
F-3-2-5	0.01	10.88	0.05	0.37	0.54	0.30	1.15	0.34	3.70	1.46	6.83	1.93	24.31	5.56	62.54	1.13	57.43
F-3-2-9	0.01	6.88	0.01	0.10	0.11	0.08	0.33	0.07	0.90	0.35	1.63	0.52	6.80	1.93	152.48	1.19	19.74
F-3-2-11	0.01	84.38	1.74	12.10	6.48	2.68	10.59	1.92	16.57	4.99	20.57	5.34	61.74	14.16	15.02	0.98	243.27
F-3-2-16	0.07	27.91	0.41	1.65	0.67	0.28	1.04	0.16	1.33	0.33	1.53	0.41	5.45	1.61	19.78	1.02	42.84
F-3-2-17	0.51	311.38	33.34	152.94	40.17	13.76	28.73	4.10	26.44	5.96	19.25	4.15	43.86	8.65	2.88	1.18	693.24
F-3-2-19	0.01	11.49	0.08	0.49	0.70	0.26	2.13	0.57	7.07	2.74	13.70	3.72	44.66	10.11	42.46	0.60	97.74
F-3-2-20	0.00	19.02	0.10	0.69	0.61	0.53	1.06	0.28	3.06	1.05	5.10	1.47	19.15	4.77	59.05	2.00	56.88
F-3-2-21	0.00	8.79	0.02	0.31	0.28	0.28	0.90	0.29	3.29	1.27	5.89	1.83	23.49	5.73	136.45	1.55	52.37
F-3-2-22	0.00	8.90	0.03	0.31	0.34	0.18	1.11	0.27	3.43	1.45	7.64	2.33	29.90	7.39	92.10	0.81	63.27
F-3-2-23	0.00	20.78	0.09	0.69	0.49	0.39	1.15	0.28	2.77	0.96	4.55	1.36	16.52	4.21	71.68	1.53	54.23
F-3-2-25	0.00	20.42	0.13	0.83	0.69	0.34	2.48	0.59	6.89	2.74	13.17	3.70	41.70	9.04	48.77	0.71	102.72
F-3-2-26	0.00	49.59	0.56	3.30	1.23	0.49	1.49	0.25	2.23	0.62	2.49	0.75	9.22	2.46	27.49	1.11	74.69
F-3-2-27	0.00	30.94	0.24	1.24	0.77	0.37	1.39	0.36	3.18	1.13	5.05	1.30	16.68	4.44	40.02	1.08	67.09
F-3-2-29	0.00	7.61	0.02	0.20	0.34	0.23	0.99	0.30	3.09	1.06	5.58	1.70	21.13	5.44	118.13	1.13	47.69
F-3-2-30	0.00	11.91	0.04	0.22	0.30	0.22	0.66	0.17	2.13	0.78	3.73	1.10	13.67	3.34	92.44	1.47	38.29
F-3-2-32	0.01	24.05	0.92	5.57	3.00	1.92	4.00	0.73	6.33	1.99	9.88	2.82	36.22	9.40	8.08	1.69	106.84
F-3-2-33	0.00	11.38	0.05	0.29	0.42	0.17	1.89	0.59	8.05	3.46	18.80	5.82	67.27	14.78	70.66	0.49	132.96
F-3-2-34	0.00	13.05	0.08	0.33	0.29	0.26	0.71	0.18	2.23	0.71	3.34	1.02	13.83	3.24	50.64	1.68	39.26

Table 1. *Cont.*

	La	Ce	Pr	Nd	Sm	Eu	Gd	Tb	Dy	Ho	Er	Tm	Yb	Lu	Ce/Ce* [1]	Eu/Eu* [2]	REE
F-3-2-36	0.00	10.86	0.07	0.30	0.19	0.09	0.33	0.04	0.50	0.18	0.76	0.22	3.31	0.99	48.17	1.09	17.85
F-3-2-37	0.00	28.29	0.33	1.84	0.77	0.25	1.01	0.14	1.17	0.35	1.31	0.38	5.72	1.64	26.61	0.87	43.19
F-3-2-38	0.01	12.47	0.09	0.57	0.32	0.15	0.49	0.11	0.96	0.36	1.62	0.46	5.93	1.56	41.18	1.16	25.09
F-4-3	0.02	41.17	0.24	1.81	1.86	1.27	8.28	2.51	32.88	14.05	73.85	20.74	232.42	50.02	51.53	0.83	481.13
F-4-6	0.02	96.94	0.29	2.13	3.13	1.93	17.95	6.59	91.47	40.31	207.09	55.58	594.13	119.40	100.99	0.62	1236.95
F-4-7	0.00	51.99	0.13	1.20	2.28	1.26	9.09	2.65	35.54	14.91	75.78	20.71	233.04	48.62	124.16	0.73	497.21
F-4-8	0.00	64.73	0.20	2.09	3.06	1.66	10.95	3.72	46.81	19.24	98.15	27.22	292.49	61.48	100.48	0.78	631.78
F-4-10	0.00	20.55	0.56	3.77	3.32	2.62	8.82	2.34	27.96	10.39	51.11	13.97	153.24	32.44	11.39	1.40	331.10
F-4-11	0.00	99.55	0.30	3.98	5.95	3.10	21.20	6.95	92.73	39.76	201.94	55.21	578.42	115.49	103.02	0.75	1224.58
F-4-13	0.01	51.28	1.41	10.71	5.99	3.87	12.83	2.98	30.59	10.73	49.97	13.62	162.65	36.40	11.26	1.31	393.04
F-4-15	0.00	45.19	0.24	1.72	1.99	1.26	6.98	2.13	27.94	11.43	59.99	16.79	188.76	40.64	58.46	0.92	405.07
F-4-16	0.00	39.11	0.28	1.58	2.48	1.65	8.05	2.65	35.79	15.68	81.52	22.61	255.69	54.58	43.36	1.03	521.66
F-4-19	0.00	179.07	0.82	7.68	9.14	4.92	31.73	8.92	104.30	39.89	183.34	46.66	472.17	93.64	67.80	0.79	1182.28
F-4-23	0.00	75.54	0.26	2.45	3.66	1.97	15.91	5.69	72.70	31.41	167.54	46.05	515.49	108.60	90.20	0.67	1047.27
F-4-25	0.00	271.74	0.40	3.66	9.01	7.38	63.44	26.74	393.79	174.04	866.55	234.31	2498.54	439.31	210.91	0.69	4988.91
F-4-29	0.00	85.67	0.25	2.32	3.46	2.01	16.07	5.97	81.49	35.89	182.21	48.87	527.81	108.97	106.39	0.69	1101.00
F-4-30	0.00	94.50	0.24	2.27	2.74	2.00	15.26	6.01	83.62	36.60	187.08	51.09	564.86	114.64	122.24	0.75	1160.92
F-4-32	0.00	207.42	0.85	9.12	11.57	5.84	45.11	13.85	173.90	71.23	341.14	87.03	872.23	166.77	75.76	0.68	2006.06
F-5-1	0.00	12.25	0.10	1.21	2.94	0.22	13.62	4.86	63.30	25.28	115.16	28.62	281.04	52.29	38.03	0.09	600.88
F-5-6	0.00	28.89	0.11	1.49	2.21	0.18	9.65	3.10	39.87	14.66	65.72	16.08	157.98	28.29	81.54	0.10	368.22
F-5-10	0.00	25.03	0.09	1.11	2.23	0.20	8.74	3.00	36.02	13.11	59.51	14.56	139.28	26.04	86.34	0.12	328.92
F-5-17	0.00	23.53	0.19	1.58	2.63	0.13	14.93	5.78	76.75	30.30	134.95	32.13	302.44	52.56	38.45	0.05	677.88
F-5-22	0.00	38.93	0.26	2.53	4.18	0.45	15.91	5.92	73.33	27.88	133.53	36.21	380.36	72.02	46.49	0.15	791.51
F-5-23	0.00	34.89	0.16	1.54	2.66	0.18	11.73	4.14	52.20	19.51	90.04	22.35	216.03	39.69	67.70	0.08	495.13
F-5-26	0.00	25.25	0.12	1.28	3.05	0.09	14.60	5.82	73.42	28.21	128.55	31.00	287.86	51.43	65.33	0.03	650.69
F-5-28	0.01	24.52	0.29	2.84	4.23	0.83	18.25	6.44	74.00	26.89	108.27	23.40	216.45	37.59	25.89	0.25	544.01
F-5-32	0.01	32.42	0.51	3.49	7.84	0.65	32.03	11.05	134.30	47.91	196.92	41.78	355.52	58.92	19.58	0.11	923.36
F-5-33	0.00	20.53	0.15	1.41	2.70	0.20	13.68	4.30	51.32	17.63	70.80	15.74	138.07	23.95	42.49	0.08	360.50
F-5-34	0.00	22.08	0.16	1.50	3.48	0.30	16.42	5.22	64.23	21.74	88.65	18.60	172.84	29.36	42.84	0.10	444.59
F-5-35	0.03	40.89	1.12	5.62	7.92	1.70	31.51	12.09	156.39	60.06	270.51	65.96	629.05	109.11	11.21	0.29	1391.96

[1] Ce/Ce* = $2 \times \frac{Ce_N}{La_N + Pr_N}$. [2] Eu/Eu* = $2 \times \frac{Eu_N}{Sm_N + Gd_N}$. Values are normalized by the C1 chondritic data from Sun and McDonough [50].

Table 2. LA-ICP-MS zircon U–Pb dating results of samples in Zhangjiakou-Xuanhua area.

Measuring Point Number	U	Th	Th/U	Isotope Ratio ± 1σ						Age (Ma)						%U–Pb disc *
				^{207}Pb/^{206}Pb		^{207}Pb/^{235}U		^{206}Pb/^{238}U		^{207}Pb/^{206}Pb		^{207}Pb/^{235}U		^{206}Pb/^{238}U		
				Ratio	1σ	Ratio	1σ	Ratio	1σ	Age	1σ	Age	1σ	Age	1σ	
D-9-07	622.2	526.0	0.85	0.0552	0.0006	0.4775	0.0072	0.0626	0.0007	420.42	22.22	396.34	4.97	391.60	4.55	1.21
D-9-08	77.3	526.0	0.16	0.0577	0.0014	0.4934	0.0127	0.0624	0.0011	520.41	53.70	407.25	8.67	390.45	6.48	4.30
D-9-10	179.5	12.0	0.40	0.0535	0.0011	0.4612	0.0110	0.0625	0.0007	350.06	46.29	385.11	7.63	391.03	4.54	1.51
D-9-11	86.0	71.4	0.17	0.0557	0.0016	0.4782	0.0129	0.0629	0.0010	438.94	62.96	396.87	8.86	393.10	6.28	0.96
D-9-13	32.4	14.9	0.10	0.0570	0.0019	0.4846	0.0171	0.0619	0.0010	500.04	75.92	401.25	11.70	387.45	6.32	3.56
D-9-16	346.1	3.2	0.66	0.0565	0.0009	0.4969	0.0126	0.0636	0.0012	472.27	33.33	409.63	8.55	397.33	7.02	3.10
D-9-18	374.7	228.5	0.31	0.0559	0.0007	0.4798	0.0090	0.0624	0.0010	455.60	29.63	397.95	6.18	389.94	5.85	2.05
D-9-21	502.7	117.7	0.98	0.0547	0.0006	0.4650	0.0075	0.0617	0.0008	398.20	22.22	387.72	5.17	385.75	4.83	0.51
D-9-23	431.2	490.7	0.36	0.0551	0.0007	0.4652	0.0074	0.0612	0.0006	416.72	34.26	387.85	5.14	382.78	3.44	1.33
D-9-31	232.3	156.7	0.19	0.0537	0.0008	0.4596	0.0086	0.0620	0.0008	366.72	33.33	383.99	6.00	387.73	4.56	0.96
D-9-32	274.5	43.6	0.09	0.0561	0.0009	0.4896	0.0113	0.0631	0.0009	457.45	39.81	404.67	7.73	394.39	5.50	2.61
F-2-05	1609.7	993.0	0.62	0.0507	0.0006	0.1418	0.0024	0.0202	0.0002	227.85	23.14	134.69	2.12	129.07	1.47	4.35
F-2-08	2029.2	1497.0	0.74	0.0499	0.0005	0.1556	0.0024	0.0226	0.0003	190.82	25.92	146.88	2.12	144.34	2.03	1.76
F-2-12	1885.8	1273.5	0.68	0.0514	0.0006	0.1606	0.0030	0.0226	0.0003	257.47	25.92	151.19	2.63	144.25	2.14	4.81
F-2-20	1550.7	904.8	0.58	0.0496	0.0005	0.1555	0.0025	0.0227	0.0003	176.01	22.22	146.71	2.19	144.80	1.96	1.32
F-2-21	1978.0	2077.8	1.05	0.0505	0.0006	0.1562	0.0027	0.0224	0.0003	220.44	32.40	147.35	2.35	142.58	1.74	3.34
F-2-22	1792.7	1177.1	0.66	0.0504	0.0006	0.1420	0.0020	0.0204	0.0002	213.04	25.92	134.79	1.81	130.21	1.33	3.51
F-2-27	1940.7	1471.4	0.76	0.0491	0.0005	0.1521	0.0022	0.0224	0.0003	153.79	24.07	143.78	1.94	143.07	1.62	0.50
F-2-32	2251.9	2236.8	0.99	0.0497	0.0005	0.1528	0.0025	0.0223	0.0003	188.97	28.70	144.36	2.21	141.93	1.76	1.71
F-2-34	909.5	942.9	1.04	0.0490	0.0008	0.1485	0.0026	0.0220	0.0002	146.38	38.89	140.60	2.30	140.05	1.11	0.39
F-2-39	790.6	738.2	0.93	0.0508	0.0007	0.1563	0.0030	0.0223	0.0003	231.55	31.47	147.43	2.61	142.05	1.64	3.79
F-2-45	1031.0	691.5	0.67	0.0499	0.0008	0.1537	0.0029	0.0223	0.0003	190.82	39.81	145.20	2.52	142.40	1.70	1.96
F-3-2-04	373.5	96.5	0.26	0.0544	0.0007	0.4524	0.0077	0.0604	0.0008	387.09	25.00	378.95	5.42	377.84	5.09	0.29
F-3-2-05	357.7	91.7	0.26	0.0538	0.0006	0.4394	0.0078	0.0591	0.0009	364.87	23.15	369.85	5.53	370.33	5.31	0.13
F-3-2-09	66.0	15.4	0.23	0.0538	0.0016	0.4392	0.0136	0.0591	0.0008	364.87	64.81	369.68	9.57	370.24	4.85	0.15
F-3-2-11	578.9	258.3	0.45	0.0538	0.0007	0.4415	0.0072	0.0592	0.0007	364.87	23.15	371.33	5.08	370.77	4.07	0.15
F-3-2-16	375.8	124.2	0.33	0.0535	0.0006	0.4488	0.0069	0.0607	0.0008	350.06	25.93	376.42	4.83	379.98	4.91	0.94
F-3-2-17	1002.3	857.5	0.86	0.0537	0.0005	0.4564	0.0062	0.0615	0.0007	366.72	15.74	381.78	4.35	384.72	4.48	0.76
F-3-2-19	435.4	128.0	0.29	0.0534	0.0006	0.4447	0.0070	0.0603	0.0007	342.65	24.07	373.55	4.94	377.31	4.39	0.99
F-3-2-20	543.5	164.7	0.30	0.0535	0.0007	0.4339	0.0083	0.0588	0.0009	346.35	27.78	365.94	5.87	368.37	5.76	0.66
F-3-2-21	204.0	53.1	0.26	0.0530	0.0010	0.4306	0.0093	0.0589	0.0008	331.54	42.59	363.57	6.62	368.96	5.02	1.46
F-3-2-22	45.9	12.6	0.27	0.0553	0.0016	0.4632	0.0156	0.0607	0.0010	433.38	58.33	386.51	10.82	379.64	5.78	1.81
F-3-2-23	468.6	111.0	0.24	0.0532	0.0006	0.4597	0.0084	0.0627	0.0010	344.50	25.92	384.06	5.88	392.11	5.88	2.05
F-3-2-25	534.8	359.8	0.67	0.0534	0.0007	0.4663	0.0069	0.0633	0.0006	346.35	27.78	388.61	4.77	395.71	3.66	1.79
F-3-2-26	693.8	293.5	0.42	0.0535	0.0005	0.4649	0.0072	0.0631	0.0008	350.06	22.22	387.68	4.97	394.16	5.04	1.64
F-3-2-27	401.2	105.2	0.26	0.0529	0.0006	0.4556	0.0079	0.0624	0.0008	324.13	25.92	381.17	5.48	389.98	4.87	2.26
F-3-2-29	199.6	49.9	0.25	0.0551	0.0009	0.4698	0.0106	0.0618	0.0010	416.72	32.41	391.08	7.35	386.67	6.24	1.14
F-3-2-30	319.8	92.2	0.29	0.0554	0.0007	0.4714	0.0089	0.0616	0.0008	427.83	-4.63	392.18	6.17	385.54	5.13	1.72

Table 2. *Cont.*

Measuring Point Number	U	Th	Th/U	Isotope Ratio ± 1σ						Age (Ma)						%U–Pb disc *
				^{207}Pb/^{206}Pb		^{207}Pb/^{235}U		^{206}Pb/^{238}U		^{207}Pb/^{206}Pb		^{207}Pb/^{235}U		^{206}Pb/^{238}U		
				Ratio	1σ	Ratio	1σ	Ratio	1σ	Age	1σ	Age	1σ	Age	1σ	
F-3-2-32	206.7	77.9	0.38	0.0527	0.0009	0.4309	0.0087	0.0594	0.0008	322.28	37.03	363.82	6.18	372.25	4.66	2.26
F-3-2-33	397.2	136.8	0.34	0.0537	0.0006	0.4574	0.0073	0.0619	0.0007	366.72	25.92	382.44	5.06	386.93	4.42	1.16
F-3-2-34	294.2	59.1	0.20	0.0522	0.0009	0.4485	0.0100	0.0622	0.0008	294.51	43.52	376.24	7.02	389.25	4.76	3.34
F-3-2-36	111.3	25.1	0.23	0.0520	0.0011	0.4344	0.0107	0.0606	0.0008	287.10	48.15	366.29	7.57	379.20	4.95	3.41
F-3-2-37	385.6	131.9	0.34	0.0525	0.0008	0.4412	0.0073	0.0611	0.0006	305.62	2.78	371.11	5.17	382.07	3.74	2.87
F-3-2-38	135.6	32.2	0.24	0.0532	0.0010	0.4410	0.0102	0.0602	0.0008	344.50	44.44	370.98	7.22	376.75	4.87	1.53
F-4-03	121.2	54.3	0.45	0.0547	0.0010	0.4513	0.0104	0.0597	0.0008	466.71	38.89	378.20	7.26	374.05	4.67	1.11
F-4-06	191.1	112.1	0.59	0.0556	0.0010	0.4664	0.0105	0.0608	0.0008	438.94	38.89	388.69	7.30	380.19	4.64	2.23
F-4-07	195.1	135.3	0.69	0.0549	0.0010	0.4567	0.0092	0.0605	0.0008	405.61	45.37	381.99	6.42	378.50	4.69	0.92
F-4-08	241.9	156.8	0.65	0.0533	0.0008	0.4371	0.0081	0.0595	0.0007	342.65	35.18	368.22	5.71	372.65	4.03	0.01
F-4-10	140.6	43.8	0.31	0.0537	0.0012	0.4431	0.0114	0.0598	0.0008	366.72	48.14	372.41	8.02	374.48	4.97	0.01
F-4-11	231.4	141.2	0.61	0.0561	0.0012	0.4708	0.0104	0.0609	0.0006	453.75	48.14	391.72	7.20	381.27	3.89	2.74
F-4-13	295.6	112.5	0.38	0.0552	0.0008	0.4593	0.0083	0.0603	0.0006	416.72	35.18	383.79	5.76	377.56	3.43	1.65
F-4-15	238.8	88.6	0.37	0.0552	0.0008	0.4594	0.0071	0.0605	0.0007	420.42	31.48	383.81	4.91	378.95	4.51	1.28
F-4-16	237.8	62.9	0.26	0.0550	0.0010	0.4771	0.0117	0.0628	0.0011	413.01	40.74	396.08	8.04	392.44	6.38	0.93
F-4-19	542.1	809.5	1.49	0.0538	0.0007	0.4664	0.0079	0.0627	0.0008	361.17	29.63	388.69	5.50	392.27	4.79	0.01
F-4-23	185.5	104.6	0.56	0.0552	0.0011	0.4776	0.0097	0.0629	0.0010	420.42	42.59	396.44	6.65	393.00	5.89	0.88
F-4-25	1471.7	484.3	0.33	0.0544	0.0005	0.4542	0.0053	0.0604	0.0005	387.09	20.37	380.23	3.74	378.24	3.34	0.53
F-4-29	187.4	99.4	0.53	0.0549	0.0010	0.4784	0.0097	0.0631	0.0007	409.31	40.74	396.99	6.69	394.55	4.35	0.62
F-4-30	211.4	117.7	0.56	0.0556	0.0009	0.4829	0.0117	0.0629	0.0011	435.23	39.81	400.06	7.99	393.27	6.85	1.73
F-4-32	472.9	781.7	1.65	0.0543	0.0008	0.4534	0.0074	0.0605	0.0005	388.94	31.48	379.66	5.19	378.64	3.08	0.27
F-5-01	300.2	109.9	0.37	0.1529	0.0013	9.7182	0.1778	0.4597	0.0072	2388.89	13.73	2408.43	16.92	2438.05	31.78	2.02
F-5-06	79.7	34.6	0.43	0.1112	0.0013	4.9839	0.0849	0.3249	0.0045	1820.37	22.22	1816.60	14.46	1813.85	22.02	0.36
F-5-10	57.0	24.4	0.43	0.1114	0.0014	5.0494	0.1071	0.3283	0.0052	1833.34	28.55	1827.65	18.01	1830.10	25.16	0.18
F-5-17	600.3	148.0	0.25	0.1558	0.0011	9.7485	0.1381	0.4540	0.0064	2410.19	11.72	2411.30	13.14	2412.98	28.35	0.12
F-5-22	378.7	334.3	0.88	0.1630	0.0012	10.4126	0.1752	0.4621	0.0064	2487.35	11.89	2472.17	15.68	2448.96	28.05	1.57
F-5-23	134.4	58.9	0.44	0.1125	0.0010	5.0599	0.0845	0.3257	0.0048	1840.43	16.21	1829.41	14.22	1817.58	23.16	1.26
F-5-26	478.7	71.0	0.15	0.1608	0.0011	10.0577	0.1207	0.4530	0.0046	2464.81	10.65	2440.10	11.21	2408.50	20.61	2.34
F-5-28	34.9	79.2	2.27	0.1168	0.0021	5.4045	0.2919	0.3296	0.0131	1909.26	32.26	1885.57	46.30	1836.20	63.38	3.98
F-5-32	120.6	86.2	0.71	0.1593	0.0013	10.0487	0.1305	0.4565	0.0048	2450.00	13.73	2439.27	12.11	2424.17	21.49	1.07
F-5-33	29.0	35.6	1.23	0.1151	0.0018	5.1916	0.1290	0.3268	0.0065	1883.34	27.93	1851.24	21.19	1822.86	31.76	3.32
F-5-34	38.2	47.0	1.23	0.1181	0.0023	5.4222	0.3277	0.3253	0.0144	1928.71	36.27	1888.38	51.82	1815.48	70.23	6.24
F-5-35	781.8	211.0	0.27	0.1623	0.0011	10.1501	0.1311	0.4529	0.0055	2479.93	11.12	2448.55	12.05	2408.09	24.46	2.98

* If the age of ^{206}Pb/^{238}U is no less than 1000 Ma, %U–Pb disc = $\left(\frac{^{207}\mathrm{Pb}/^{206}\mathrm{Pb}}{^{206}\mathrm{Pb}/^{238}\mathrm{U}} - 1\right) \times 100$. Otherwise, %U–Pb disc = $\left(\frac{^{207}\mathrm{Pb}/^{235}\mathrm{U}}{^{206}\mathrm{Pb}/^{238}\mathrm{U}} - 1\right) \times 100$.

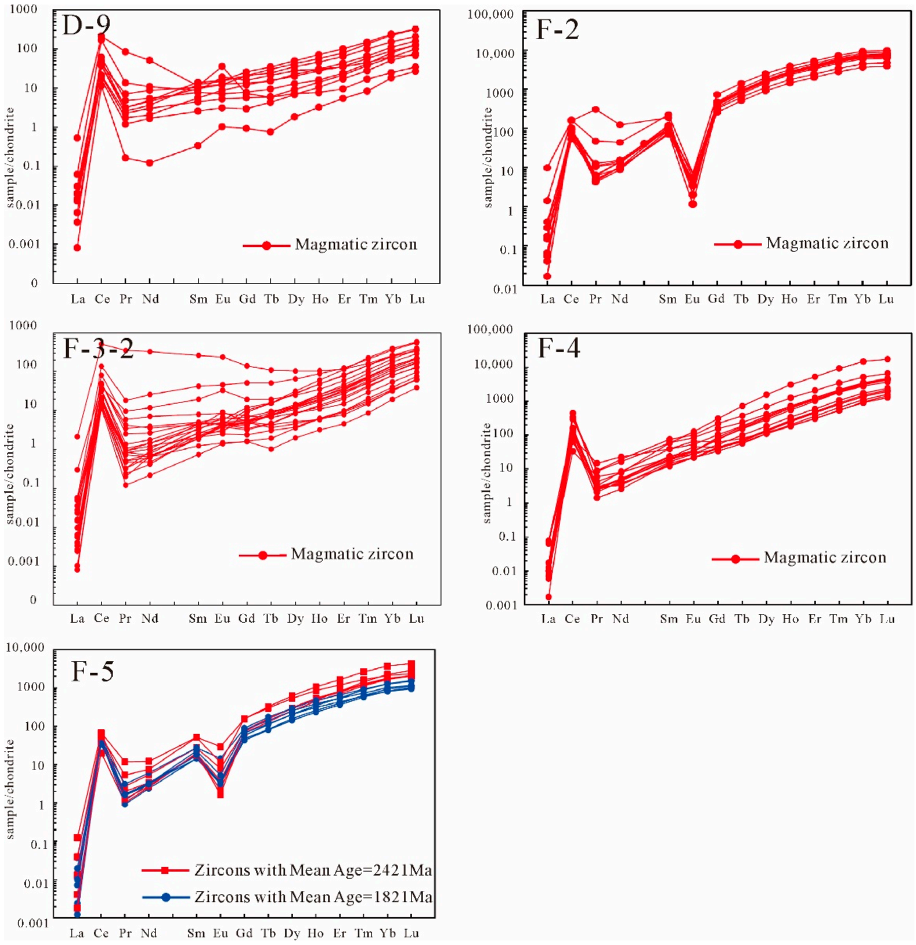

Figure 7. Chondrite normalized REE patterns of zircons from samples (by the GeoKit program [51] with C1 chondritic data from Sun and McDonough [50]).

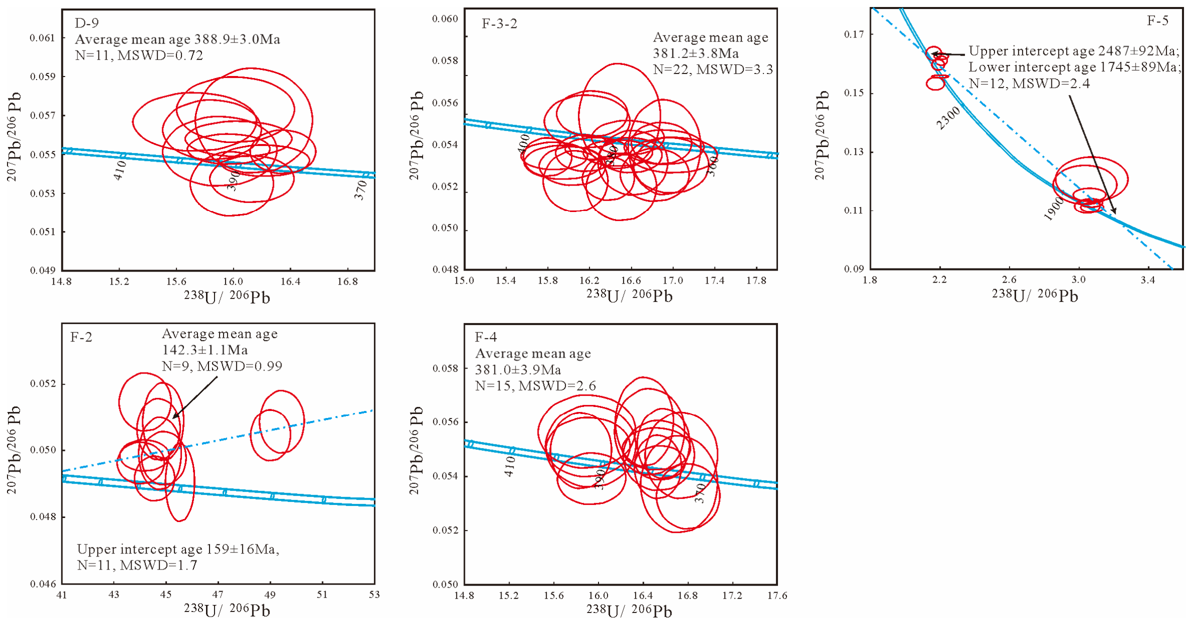

Figure 8. U–Pb inverse Concordia (Terra Wasserburg) plots for zircon from samples in the Zhangjiakou-Xuanhua area.

We double-dated these three samples from the SQG complex with U–Pb and ZFT to constrain the post-magmatic thermal history. The ZFT ages exhibit a narrow range from 95 ± 6 Ma to 68 ± 20 Ma. Sample chi-square values (Table 3) are higher than 5%, consistent with normal Poisson distributions. The ZFT ages are significantly younger than the forming ages of the SQG complex recorded in previous studies, suggesting that the ZFT ages may represent the cooling ages of the SQG complex.

Table 3. Fission-track ages of zircon from the Zhangjiakou-Xuanhua area using an external detector method and zeta calibration approach.

Sample /Mineral	n	Spontaneous $\rho_s(N_s)$ [1]	Induced $\rho_i(N_i)$	Dosimeter $\rho_d(N_d)$	$P(\chi^2)$ [2] (%)	Central Age Ma (±1σ) [3]	Pooled Age Ma (±1σ)
D-9	2	84.29 (116)	9.446 (13)	1.735 (1253)	98.4	68 ± 20	68 ± 20
F-2	3	86.47 (289)	11.37 (38)	2.316 (1253)	95.4	77 ± 14	77 ± 14
F-3-2	17	97.222 (2265)	12.319 (287)	2.164 (1253)	92.6	75 ± 6	75 ± 6
F-4	40	102.107 (7849)	9.431 (725)	2.013 (1253)	100.0	95 ± 6	95 ± 6
F-5	35	103.218 (8249)	5.393 (431)	1.861 (1253)	98.9	155 ± 10	155 ± 10

[1] Track densities (ρ) are as measured and are (10^5 per cm^{-2}); number of grains counted (n) are shown in parentheses. [2] $P(\chi^2)$ is chi-square probability. [3] Ages calculated with ζ (zeta) = 88.2 ± 2.9 (yr cm^2/tr).

4.2. The Shangshuiquan Granite Pluton

Sample F-2 was collected from the drilling core in the SSQ granite pluton, which intrudes into the Archaean Chongli Group metamorphic basement, the SQG alkaline complex, and the Jurassic Zhangjiakou Formation volcano-sedimentary sequence. Zircon grains separated from F-2 are euhedral and stubby prisms (<150 μm) exhibiting ambiguous oscillatory-zoning cores rounded by the bright outer rings on CL images (Figure 6). They present the development of irregular domains cutting discordantly across growth zoned domains. These domains are thought to have been developed by recrystallization [48]. The REE concentrations of zircon grains in F-2 vary between 1574 and 4127 ppm (Table 1) with significant Ce and Eu anomalies, showing typical characteristics of magmatic zircons in granite. Zircon grains from F-2 exhibit a relatively high Th and U content, with the Th/U ratio ranging from 0.58 to 1.05 (Table 2). Based on the character of the REE patterns (Figure 7), the rims do not differ in any way from the central parts of the grains. Considering the morphology, CL image, and REE signatures, it is proposed that the zircon grains in F-2 are magmatic zircons. The higher Th, U, and REE content, as well as the core-round structures in CL images, are likely results of the late-magmatic from residual melts. Two LA-ICPMS U–Pb analyses of zircon grains on rims demonstrated remarkable discordant ages (Figure 8), indicating the disturbed U–Pb system. Nine spots on cores yielded a weighted average age of 142.3 ± 1.1 Ma (MSWD = 0.99), representing the crystallization age of the SSQ granite pluton.

ZFT dating was also carried out upon the sample F-2, but only three efficient zircon grains were obtained with a high chi-square value of 95.4% (Table 3). Therefore, the central ZFT age of 77 ± 14 Ma, approximately 65 Ma younger than the sample's zircon U–Pb age, represents SSQ granite pluton's cooling age in the Late Cretaceous, which indicates the resetting time when the sample F-2 is cooling through the closure temperature of the ZFT (200–250 °C).

4.3. The Xiaoyingpan Ore-Bearing Quartz Veins

Sample F-5 was taken from altered ore-bearing K-feldspathic quartz veins in the Xiaoyingpan gold deposit. Zircon grains from F-5 are mostly round in shape (<200 μm), suggesting an alteration in later metamorphism. These zircons record domains with oscillatory zoning generated by dissolution/re-precipitation or crystallization in the presence of melts [52–54], together with lobate structureless grey or luminescent rims invading older cores (metamorphic re-crystallization in [48]) (Figure 6). However, some of the edges are too narrow to date. The REE concentrations of the zircon grains obtained in F-5 vary between 329 and 1392 ppm (Table 1), showing LREE depleted chondrite normalized REE patterns (Figure 7). Thorium and uranium contents of zircon from sample F-5 vary between 24.4 and 420 ppm and 29.0–782 ppm, respectively, with Th/U ratios of 0.15–2.27. Most occurrences of metamorphic zircon with Th/U > 0.1 (with values as high as 3.) are from high and ultra-high temperature (> 900 °C) samples [55–59]. The U–Pb results fall along a discordant line on the Concordia diagram (Figure 8). This line yields an upper intercept at 2487 ± 92Ma and a lower intercept at 1745 ± 89Ma (MSWD = 2.4). The upper intercept age probably records the crystallization ages of the inherited cores, whereas the lower intercept age might indicate an ultra-high temperature metamorphic event.

The ZFT central ages of F-5 were dated as 155 ± 10 Ma by analyzing 35 zircon grains with a high chi-square value of 98.9%. Since the significant inconsistency between the zircon U–Pb and ZFT ages, the ZFT age of 155 ± 10 Ma is interpreted as the cooling age of the ore-bearing K-feldspathic quartz veins in the Xiaoyingpan gold deposit.

5. Discussion

5.1. Geochronology Constraints on Intrusions and the Cooling History

Due to the different isotopic closure temperatures of K-Ar, Ar-Ar, and Rb-Sr dating method systems, there is great controversy concerning the formation and emplacement ages of the SQG alkaline complex. In general, the closure temperatures of these systems are lower than that of magma crystallization. High-temperature chronometers (e.g., U/Pb, ^{40}Ar/^{39}Ar from hornblende or biotite) collected from within an intrusion often reflect the cooling age of the intrusion and represent the inherited or parent age of a pluton [60]. The zircon U–Pb ages, with the closure temperature of approximately 750 °C, are often used to detect the ages of magma emplacement because its closure temperature is relatively close to that of magma crystallization, while the low-temperature thermochronometers give constraints on post-emplacement information in general.

F-3-2 and F-4 collected in this paper are from fresh K-feldspar pegmatite and alternated K-feldspar pegmatite in the ZZL area, respectively. Their zircon grains yielded a wide range of ages between 376 and 393 Ma. The elder ages are consistent with the age of altered cataclasite (D-9, 388.9 ± 3.0 Ma) in addition to gold-bearing quartz veins in the Dongping gold deposit. It is probably that the later tectonic movement had crushed the rocks in the SQG complex to form the cataclasite, which contained the zircon grains from the SQG complex. Furthermore, according to the dating of different parts of the SQG complex, similar zircon U–Pb ages have been reported in recent years, ranging from 390 Ma to 386 Ma [30]. Thus, 388.9 ± 3.0 Ma represents the crystalline age of the SQG alkaline complex.

The porphyritic granite cutting through the K-feldspar pegmatite in the ZZL was dated as 373.0 ± 3.5 Ma [35], which indicates the characteristics of multi-stage magmatism of the SQG complex. Pegmatite is usually formed in the late stage of magmatism due to its abundant volatility. Therefore, the younger zircon grains in F-3-2 and F-4 probably represent the forming ages of different pegmatite dikes in the ZZL area and reveal that magmatic-hydrothermal activities were still present and active after the emplacement of the SQG alkaline magma. Since the early Paleozoic period, the subduction of the Paleo-Asian Ocean plate beneath the NCC has resulted in the metamorphic dehydration of the lithospheric mantle [61–63]. From the Early Devonian to the Late Permian period, the collision between the Siberian plate and the NCC has led to widespread magmatism along the deep fault zones in the northern margin of the NCC. The SQG alkaline complex was regionally formed along the SCD fault in the post-collisional extensional tectonic background [64].

The 327 ± 9 Ma hornblende Ar-Ar age and 327–260 Ma whole-rock Rb-Sr ages for the SQG complex were once interpreted as the emplacement age of the complex. However, combined with our dating results and the closure temperatures of the chronometers, the Ar-Ar age is the cooling age of the SQG complex, revealing the cooling history of the complex after emplacement [30].

The K-Ar ages of the SQG complex are 257–126 Ma, with a peak between 230 Ma and 170 Ma, which are younger than the Ar-Ar and U–Pb ages; 230 Ma is close to the emplacement age of the Guzuizi rock mass on the south side of the rock mass (236 Ma [30]), thus 230 Ma may be the reset age of the SQG complex affected by the intrusion of the Guzuizi pluton. The previous K-Ar age of 140 Ma is highly consistent with U–Pb ages of cores in zircon grains from F-2. In addition, Miao et al. [30] obtained the magmatic zircon U–Pb age of 142 Ma from the SSQ pluton and interpreted it as the emplacement age. Therefore, it is likely that the emplacement of the SSQ pluton in 142 Ma reheated the SQG complex and reset the K-Ar ages. This reheating time of the SQG complex is consistent with the Yanshanian metallogenetic ages of gold deposits within the SQG complex [3,13,19,35,65]. The regional early Cretaceous granitic magmatism coincided with the widespread Jurassic-Cretaceous volcanism and magmatism in eastern China caused by rifting events in the Yanshanian orogeny [66,67]. Widespread mafic microgranular enclaves hosted in the Late-Jurassic to the Early Cretaceous granitoid intrusions in the eastern NCC indicate the lithospheric extension [65]. The granulitic xenoliths hosted in Hannuoba basalt (ca. 140 Ma) in Chengde (north of the study area) prove that mantle-derived basaltic melt already underplated the lower crust in the Late Jurassic period [30,68,69]. The SSQ granite was classified as A-type granite with relatively low Al_2O_3 and MgO and significant Eu depletion in the previous study [28]. Thus, the SSQ granite intrusion is probably the result of the interaction between the mantle melt and the lower crust in the Late Jurassic period.

The tectonic regime of transition from compression to extension in the Early Cretaceous resulted in widespread volcanism and granite emplacement in the Zhangjiakou-Xuanhua area, including the forming of Zhangjiakou Formation (127.8 ± 3.9 Ma) and Beizhazi alkali granite (130.5 ± 1.5 Ma) [70]. The reheating caused by the emplacement of the Beizhazi granite, and the eruption of intermediate acid magmatism might reset the low temperature thermochronological ages in the study area. The ZFT ages of the samples from the SQG complex and SSQ granite yield between 95 ± 6 Ma and 68 ± 20 Ma, representing the cooling age after the reheat of magmatism in the Early Cretaceous period.

5.2. Constraints on Gold Mineralization

The metallogenic age of the Xiaoyingpan Gold deposit has been debated for decades. A Pb/Pb isochron age of 2711 ± 238 Ma for ankerite [71] and zircon U–Pb ages of 1826–1800 Ma from gold-bearing quartz veins [72] were explained as the multi-stage ages of Pre-Cambrian mineralization. However, our CL images show that the inherited or xenocrystic zircons are common in gold-bearing quartz veins. Since the ore-forming temperature is below 350 °C [73] in the Xiaoyingpan gold deposit, the mineralization will not reset the age of inherited and xenocrystic zircons. Thus, the pre-Cambrian ages probably represent the records of regional metamorphism rather than reveal a metallogenic epoch. The upper and lower intercept ages of sample F-5 are coeval with the 2.5 Ga and 1.8 Ga craton-scale events in the NCC [74]. The NCC has a prominent age peak at around 2.5 Ga [75], and the 2.6–2.5 Ga is indicated by the widespread emplacement of mantle-derived mafic igneous rocks [76]. The TTG (tonalite-trondhjemite-granodiorite) gneiss of the Late Archean units, such as the Sanggan and Chongli complex, are dated as 2520–2500Ma [77–79]. The upper intercept age (2487 ± 92Ma) is similar to the forming ages of TTG gneiss in Northwest Hebei Province and, thus, could record the age of the basement in the NCC. The gneiss-granulite rocks in the NCC have undergone widespread amphibolite-granulite facies metamorphism at about 1850~1800 Ma [80–82]. Thus, the lower intercept age (1745 ± 89Ma) could be attributed Pb loss during metamorphism.

The ZFT age of F-5 (155 ± 10 Ma) is significantly younger than the zircon U–Pb ages, therefore representing a cooling or reset age. Because the closure temperature of ZFT is lower than the ore-forming temperature of the Xiaoyingpan gold deposit, the gold deposit was formed before 155 ± 10 Ma. Miao et al. [30] inferred that the Xiaoyingpan gold deposit was formed during the Mesozoic period based on the intersection relationships between gold-bearing quartz veins and host rocks. Thus, the Xiaoyingpan gold deposit may form during the Mesozoic and earlier than 155 ± 10 Ma. The white mica Ar-Ar age of hydrothermally altered wall rock in Xiaoyingpan and whole-rock Rb-Sr ages of the Guzuizi granite is dated as 354.3–230 Ma [13] and 184 ± 24 Ma [29], respectively. The Ar-Ar age of 230 Ma is coeval with the emplacement of Guzuizi granite (236 Ma) and, thus, probably represents the reset age of Sanggan Group metamorphic host rocks in Xiaoyingpan. Furthermore, 184 ± 24 Ma may be the cooling age of Guzuizi granite. If this is the case, the Xiaoyingpan gold deposit, hosted by Sanggan Group metamorphic rock and Guzuizi granite might undergo a similar cooling history. The widespread magmatism in the early Cretaceous period did not have to reheat them to sufficient temperatures to reset the ZFT ages.

The post-magmatic hydrothermal alterations in 389–385 Ma were once treated as the main stage of gold mineralization in the Dongping deposit, and the hydrothermal event in ~140 Ma is inferred as a late-stage overprint for gold mineralization [12]. However, the latest in situ U–Pb geochronology of garnet suggested that gold mineralization at Dongping occurred in the Early Cretaceous period (142–139 Ma) [65], which is consistent with the emplacing age of the SSQ granite in this paper. Similarly, Wei et al. [35] also obtained the age of 142.0 ± 1.2 Ma from porphyritic granite within the SQG complex. The synchronous emplacement of the SSQ intrusion may be a major heat source for gold mineralization in Dongping. This is coeval with the development of metamorphic core complexes and rift basins in the eastern North China Craton caused by the lithospheric extension during the Late Jurassic to Early Cretaceous period [83–85], which resulted in the mineralization of most gold deposits in the eastern North China Craton during 140 Ma to 120 Ma [70,86–88].

The Dongping gold deposit was formed in ~140 Ma, while the mineralization of the Xiaoyingpan gold deposit ended in 155 Ma at the latest. The differences in the metallogenic epoch imply the distinctions in ore-forming heat sources. The isotopic studies of the two deposits indicate that their S and Pb isotopic compositions are similar and homologous to some extent. Both deposits and the Sanggan group show the characteristics of mantle-derived S, while the gold deposits and the SQG complex show a similar Pb isotopic composition [17,37,38,68,89,90]. The ore-forming fluids of the two deposits also show the characteristics of mixed fluids, which are neither typical magmatic water nor metamorphic water or meteoric water [11,21,89,91]. Therefore, the metallogenic systems of Xiaoyingpan and Dongping gold deposits were probably similar. The metamorphic rock of Sanggan Group and the SQG alkaline complex may provide some ore-forming materials for mineralization. Jiang Sihong et al. [24] indicated that the two deposits were formed by the filling and metasomatism of mixed hydrothermal fluid of magmatic and meteoric water into different tectonic locus under the high geothermal background after the formation of the SQG alkaline complex. The ore-forming process of Xiaoyingpan and Dongping might have been influenced by the intrusion of the Guzuizi granitoid and the SSQ granitoid, respectively. The heats of magmatic intrusion and meteoric water activate the Au, K, and Si by leaching and replacing the metamorphic rocks of the Sanggan Group or the SQG complex to form the potassium-silica-rich gold-bearing hydrothermal fluid. With the cooling of magma, the Xiaoyingpan gold deposit and Dongping gold deposit were formed by filling and metasomatism of the gold-bearing hydrothermal fluid in the metamorphic rocks of the Sanggan Group and the SQG alkaline complex, respectively.

6. Conclusions

This paper combined zircon U–Pb dating and zircon fission track dating to study the chronology of several granites and gold deposits in the Xuanhua and Chongli areas of Zhangjiakou City, northwest Hebei Province. The results have improved the understanding of regional magmatic activity and mineralization processes.

The regional basement metamorphism occurred at (2487 ± 92) Ma, followed by superimposition during (1745 ± 89) Ma, which is a record of the large-scale tectonic–metamorphic movement of NCC at 2.5 Ga and 1.8 Ga. The emplacement age of the Shuiquangou alkaline complex was dated as 388.9 ± 3.0 Ma, and the related magmatic activities may have lasted to ca 377 Ma. It was associated with the collision between the Siberian plate and the NCC in the Middle-Late Devonian period, leading to widespread intrusions along the SCD fault in the area. The SSQ granite pluton formed in 142.3 ± 1.1 Ma and was linked to the underplating event in the early Cretaceous period. The SQG complex and the SSQ granites then underwent a rapid cooling stage in the Cretaceous period under the basin-ridge extension tectonic background of the NCC. The ore-forming time of the Xiaoyingpan gold deposit is between 236 and 155 Ma, while the Dongping gold deposit was probably formed in 142 Ma. The two gold deposits were formed in a similar metallogenic system but were affected by the Guzuizi granite and the SSQ granite, respectively.

Author Contributions: Conceptualization, Y.F.; methodology, Y.F. and H.W.; field work and investigation, H.W., Y.F. and D.L.; data curation, Y.F. and W.D.; writing—original draft preparation, Y.F. and W.D. All authors have read and agreed to the published version of the manuscript.

Funding: This work is funded by Natural Science Foundation of Hebei Province (Grant No. D2020403101 and No. D2020403019); Science and Technology Project of Hebei Education Department (Grant No. ZD2020134); Opening Foundation of Hebei Key Laboratory of Strategic Critical Mineral Resource (HGU-SCMR2151), and Sci-tech Popularization project of Water Resources Department of Hebei Province (Grant No. 2021-35).

Data Availability Statement: Not applicable.

Acknowledgments: We are very grateful to the Dongping Gold Mine for its support on the data collection and field work investigation.

Conflicts of Interest: The authors declare no conflict of interest.

References

1. Wang, F.X.; Pei, R.F.; Jiang, S.H.; Qiu, H.Y.; Liu, Y.F.; Zhao, Y.Y. The progress in the study of Cu-Au (Mo) deposits related to alkaline rocks. *Geol. Bull. Chin.* **2017**, *36*, 140–153. (In Chinese with English abstract)
2. Muller, D.; Groves, D. *Potassic Igneous Rocks and Associated Gold-copper Mineralization*; Springer: Berlin/Heidelberg, Germany, 2019; pp. 101–125.
3. Li, C.M.; Deng, J.F.; Chen, L.H.; Su, S.G.; Li, H.M.; Hu, S.L. Two periods of zircon from Dongping gold deposit in Zhangjiakou–Xuanhua area, northern margin of North China: Constraints on metallogenic chronology. *Miner. Depos.* **2010**, *29*, 265–275. (In Chinese with English abstract)
4. Miao, L.C.; Zhai, Y.S.; Zhu, C.W.; Guan, K.; Qiu, Y.S.; Luo, Z.K. Study on chronology of the Shuiquangou alkali complex in northwestern Hebei province, P.R. China. *Gold Geol.* **2001**, *7*, 1–6. (In Chinese with English abstract)
5. Mo, C.H.; Liang, H.Y.; Wang, X.Z.; Cheng, J.P.; Li, H.M. Zircon U-Pb dating on the alkaline complex in northwest Hebei Province. *Chin. Sci. Bull.* **1998**, *42*, 75–78. (In Chinese with English abstract)
6. Gao, S.; Xu, H.; Zhang, D.S.; Shao, H.N.; Quan, S.L. Ore petrography and chemistry of the tellurides from the Dongping gold deposit, Hebei Province, China. *Ore Geol. Rev.* **2014**, *64*, 23–34. [CrossRef]
7. Wang, D.Z.; Liu, J.J.; Zhai, D.G.; Carranza, E.J.M.; Wang, Y.H.; Zhen, S.M.; Wang, J.; Wang, J.P.; Liu, Z.J.; Zhang, F.F. Mineral paragenesis and ore-forming processes of the Dongping gold deposit, Hebei Province, China. *Resour. Geol.* **2019**, *69*, 287–313. [CrossRef]
8. Wang, M.J. Mineralization Geochemistry Features of the Dongping Gold Deposit in Chongli County, Hebei Province. Ph.D. Thesis, China University of Geosciences, Beijing, China, 2015; pp. 1–105. (In Chinese with English abstract)
9. Wei, M.H.; Chen, S.Q.; Gu, Z.F.; Yan, Y.S.; Quan, S.T. Relation between the Shuiquangou alkali intrusive complex and gold mineralization in the northwestern Hebei Province. *Miner. Expl.* **2014**, *5*, 32–38. (In Chinese with English abstract)
10. Xu, J.H.; Wei, H.; Bian, C.J.; Zhang, G.R.; Chu, H.X. Unusual Quartz Phenocrysts in a Newly Discovered Porphyritic Granite near the Giant Dongping Gold Deposit in Northern Hebei Province, China. *Acta Geosci. Sin.* **2018**, *92*, 398–399. [CrossRef]
11. Zhang, Z.C. Characteristics of H and O isotopes and fluid evolution in Dongping gold deposit. *Gold Geol.* **1996**, *2*, 36–41. (In Chinese with English abstract)
12. Bao, Z.W.; Sun, W.D.; Li, C.J.; Zhao, Z.H. U-Pb dating of hydrothermal zircon from the Dongping gold deposit in North China: Constraints on the mineralization processes. *Ore Geol. Rev.* **2014**, *61*, 107–119. [CrossRef]
13. Hart, C.J.R.; Goldfarb, R.J.; Qiu, Y.M.; Snee, L.; Miller, L.D.; Miller, M.L. Gold deposits of the northern margin of the North China Craton: Multiple late Paleozoic–Mesozoic mineralizing events. *Miner. Depos.* **2002**, *37*, 326–351. [CrossRef]
14. Li, H.M.; Li, H.K.; Lu, S.N.; Yang, C.L. Determination of age of gold mineralization of Dongping gold deposits by U-Pb dating hydrothermal zircons from ore veins. *(sup) Acta Geosci. Sin.* **1998**, *18*, 176–178. (In Chinese)
15. Jiang, S.H.; Nie, F.J. ^{40}Ar-^{39}Ar geochronology of the Shuiquangou alkaline complex and related gold deposits, Northwestern Hebei, China. *Geol. Rev.* **2000**, *46*, 621–627.

16. Lu, D.L.; Luo, X.Q.; Wang, J.J. Geochronological study on the Dongping gold deposit. *Miner. Deposits.* **1993**, *12*, 182–188. (In Chinese with English abstract)
17. Song, G.R.; Zhao, Z.H. *Geology of Dongping Alkaline Complex-Hosted Gold Deposit in Hebei Province*; Seismic Publishing House: Beijing, China, 1996; p. 181. (In Chinese with English abstract)
18. Wang, R.Z. The characteristics and genesis of the felsic alkali complex, Jinjiazhuang, Hebei. *J. Guilin Coll. Geol.* **1992**, *12*, 12–20. (In Chinese with English abstract)
19. Wang, Z.K.; Jiang, X.M.; Wang, Y.; Shang, M.Y. Origin and forming mechanism of the Shuiquangou alkaline complex in Dongping area, northwest Hebei Province, and its geological significance. *J. Precious Met. Geol.* **1992**, *1*, 18–25. (In Chinese with English abstract)
20. Xu, X.W.; Cai, X.P.; Liu, Y.L.; Zhang, B.L. Laser probe 40Ar-39Ar ages of metasomatic K-feldspar from the Hougou gold deposit, northwestern Hebei Province China. *Sci. China* **2002**, *45*, 559–564. [CrossRef]
21. Fan, H.R.; Xie, Y.H.; Zhai, M.G. Ore-forming fluids in the Dongping gold deposit, northwestern Hebei Province. *Sci. China* **2001**, *44*, 748–757. [CrossRef]
22. Mao, J.W.; Li, Y.Q.; Goldfarb, R.J.; He, Y.; Zaw, K. Fluid inclusion and noble gas studies of the Dongping gold deposit, Hebei Province, China: A mantle connection for mineralization? *Econ. Geol.* **2003**, *98*, 517–534. [CrossRef]
23. Hu, X.D.; Zhao, J.N. Geological characteristics and physico-chemical conditions for forming the Xiaoyingpan gold-bearing quartz veins in Hebei Provience. Bulletin Tianjin Institute Geol. *Min. Res.* **1984**, *11*, 39–56. (In Chinese with English abstract)
24. Jiang, S.H.; Nie, F.J. A comparison study on geological and geochemical features and ore genesis of the Xiaoyingpan and Dongping gold deposits, Hebei. *Gold Geol.* **1998**, *4*, 12–24. (In Chinese with English abstract)
25. Ren, J.S.; Jiang, C.F.; Zhang, Z.K. *Tectonics and Evolution of China*; China Science Publishing: Beijing, China, 1980; pp. 29–33. (In Chinese)
26. Hu, L.; Song, H.L.; Yan, D.P.; Hu, D.G. The $^{40}Ar/^{39}Ar$ geochronology constraint and geological significance of mylonites in Shangyi-Chicheng fault belt on the north of North China Craton. *Sci. China* **2003**, *46*, 1134–1141. [CrossRef]
27. Zhang, S.H.; Zhao, Y.; Liu, J.; Hu, J.M.; Chen, Z.L.; Pei, J.L.; Chen, Z.Y.; Zhou, J.X. Emplacement depths of the Late Paleozoic-Mesozoic grantoid intrusions from the northern North China block and their tectonic implications. *Acta Petrol. Sin.* **2007**, *23*, 625–638. (In Chinese with English abstract)
28. Zhen, S.M.; Wang, D.Z.; Bai, H.J.; Jia, R.Y.; Wang, J.; Zha, Z.J.; Li, Y.; Miao, J.P. The Paleozoic-Mesozoic magmatic-tectonic activities and their geological implications in the Zhangjiakou-Xuanhua district, northern margin of the North China Craton. *Acta Petrol. Sin.* **2021**, *376*, 1619–1652.
29. Jia, Y.F.; Li, X. Lead isotope studies of gold deposits in North China. *Miner. Depos.* **1993**, *12*, 168–173. (In Chinese with English abstract)
30. Miao, L.C.; Qiu, Y.M.; McNaughton, N.; Luo, Z.K.; Groves, D.; Zhai, Y.S.; Fan, W.M.; Zhai, M.G.; Guan, K. SHRIMP U–Pb zircon geochronology of granitoids from Dongping area, Hebei Province, China: Constraints on tectonic evolution and geodynamic setting for gold metallogeny. *Ore Geol. Rev.* **2002**, *19*, 187–204. [CrossRef]
31. Cisse, M. Geological Setting and Genesis of the Dongping Gold Deposit. Ph.D. Thesis, China University of Geosciences, Wuhan, China, 2016; 164p.
32. Lu, S.N.; Li, H.K.; Li, H.M. *Studies on Basement Characteristics and Metallogeny of the Concentrated Areas of Gold Deposits*; Geological Publishing House: Beijing, China, 1997; p. 116. (In Chinese)
33. Jiang, N.; Liu, Y.S.; Zhou, W.G.; Yang, J.H.; Zhang, S.Q. Derivation of Mesozoic adakitic magmas from ancient lower crust in the North China craton. *Geochim. Cosmochim. Acta* **2007**, *71*, 2591–2608. [CrossRef]
34. Shao, J.A.; Wei, C.J.; Zhang, L.Q.; Niu, S.Y.; Mou, B.L. Pyroxene diorite in nuclear department of Zhangxuan Uplift. *Acta Petrol. Sin.* **2004**, *20*, 1389–1396.
35. Wei, H.; Xu, J.H.; Zhang, G.R.; Cheng, X.H.; Chu, H.X.; Bian, C.J.; Zhang, Z.Y. Hydrothermal Metasomatism and Gold Mineralization of Porphyritic Granite in the Dongping Deposit, North Hebei, China: Evidence from Zircon Dating. *Minerals* **2018**, *8*, 363. [CrossRef]
36. Li, H.Y.; Zhang, Z.Y.; Li, P.; Xing, C.H. Structural analysis and genesis of gold-deposit in the Dongping. *Geol. Prospect.* **2000**, *36*, 36–38. (In Chinese with English abstract)
37. Song, R.X.; Wang, Y.Z. *Gold Deposits Geology of Hebei Province*; Geology Press: Beijing, China, 1994.
38. Wang, Z.W.; Wang, Z.H.; Zhang, Y.J.; Xu, B.; Li, Y.G.; Tian, Y.J.; Wang, Y.C.; Peng, J. Linking ~1.4–0.8 Ga volcano-sedimentary records in eastern Central Asian orogenic belt with southern Laurentia in supercontinent cycles. *Gondwana Res.* **2022**, *105*, 416–431. [CrossRef]
39. Liu, Y.S.; Hu, Z.C.; Zong, K.Q.; Gao, C.G.; Gao, S.; Xu, J.; Chen, H.H. Reappraisement and refinement of zircon U-Pb isotope and trace element analyses by LA-ICP-MS. *Chin. Sci. Bull.* **2010**, *55*, 1535–1546. [CrossRef]
40. Ludwig, K.R. *Isoplot/Ex, Version 3: A Geochronological Toolkit for Microsoft Excel: Berkeley*; Geochronology Centre: Berkeley, CA, USA, 2003.
41. Bellemans, F. Composition of SRM and CN U-doped glasses: Significance for their use as thermal neutron fluence monitors in fission track dating. *Radiat. Meas.* **1995**, *24*, 153–160. [CrossRef]
42. Gleadow, A.J.W.; Duddy, I.R.; Green, P.F.; Lovering, J.F. Confined fission track lengths in apatite: A diagnostic tool for thermal history analysis. *Contrib. Mineral. Petrol.* **1986**, *94*, 405–415. [CrossRef]

43. Hurford, A.J.; Green, P.F. A users' guide to fission track dating calibration. *Earth Planet Sci. Lett.* **1982**, *59*, 343–354. [CrossRef]
44. Hurford, A.J. Standardization of fission track dating calibration: Recommendation by the Fission Track Working Group of the IUGS Subcommission on Geochronology. *Chem. Geol.* **1990**, *80*, 171–178. [CrossRef]
45. Galbraith, R.F.; Laslett, G.M. Statistical models for mixed fission track ages. *Nucl. Tracks Radiat. Meas.* **1993**, *21*, 459–470. [CrossRef]
46. Galbraith, R.F. On statistical models for fission track counts. *Math. Geosci.* **1981**, *13*, 471–478. [CrossRef]
47. Green, P.F. A new look at statistics in fission-track dating. *Nucl. Tracks* **1981**, *5*, 77–86. [CrossRef]
48. Corfu, F.; Hanchar, J.M.; Hoskin, P.W.; Kinny, P. Atlas of zircon textures. *Rev. Mineral. Geochem.* **2003**, *53*, 469–500. [CrossRef]
49. Hoskin, P.; Schaltegger, U. The composition of zircon and igneous and metamorphic petrogenesis. *Rev. Mineral. Geochem.* **2003**, *53*, 27–62. [CrossRef]
50. Sun, S.S.; Mcdonough, W.F. Chemical and isotopic systematics of oceanic basalts: Implications for mantle composition and processes. *Geol. Soc. Lond. Spec. Publ.* **1989**, *42*, 313. [CrossRef]
51. Lu, Y.F. GeoKit—A geochemical toolkit for Microsoft Excel. *Geochimica* **2004**, *33*, 459–464. (In Chinese with English abstract)
52. Fornelli, A.; Piccarreta, G.; Micheletti, F. In situ U-Pb dating combined with SEM imaging on zircon–an analytical bond for effective geological reconstructions. In *Geochronology–Methods and Case Studies*; Books on Demand: Norderstedt, Germany, 2014; pp. 109–139.
53. Vavra, G.; Schmid, R.; Gebauer, D. Internal morphology, habit and U-Th-Pb microanalysis of amphibolite-to-granulite facies zircons: Geochronology of the Ivrea Zone (Southern Alps). *Contrib. Mineral. Petrol.* **1999**, *134*, 380–404. [CrossRef]
54. Geisler, T.; Schaltegger, U.; Tomaschek, F. Re-equilibration of zircon in aqueous fluids and melts. *Elements* **2007**, *3*, 43–50. [CrossRef]
55. Vavra, G.; Gebauer, D.; Schmidt, R.; Compston, W. Multiple zircon growth and recrystallization during polyphase Late Carboniferous to Triassic metamorphism in granulites of the Ivrea Zone (Southern Alps): An ion microprobe (SHRIMP) study. *Contrib. Mineral. Petrol.* **1996**, *122*, 337–358. [CrossRef]
56. Schaltegger, U.; Fanning, M.; Günther, D.; Maurin, J.C.; Schulmann, K.; Gebauer, D. Growth, annealing and recrystallization of zircon and preservation of monazite in high-grade metamorphism: Conventional and in-situ U–Pb isotope, cathodoluminescence and microchemical evidence. *Contrib. Mineral. Petrol.* **1999**, *134*, 186–201. [CrossRef]
57. Möller, A.; O'Brien, P.J.; Kennedy, A.; Kröner, A. Linking growth episodes of zircon and metamorphic textures to zircon chemistry: An example from the ultrahigh-temperature granulites of Rogaland (SW Norway). *Geol. Soc. Lond. Spec. Publ.* **2003**, *220*, 65–81. [CrossRef]
58. Kelly, N.; Harley, S. An integrated microtextural and chemical approach to zircon geochronology: Refining the Archean history of the Napier Complex, east Antarctica. *Contrib. Mineral. Petrol.* **2005**, *149*, 57–84. [CrossRef]
59. Rubatto, D. Zircon: The Metamorphic Mineral. *Rev. Mineral. Geochem.* **2017**, *83*, 261–295. [CrossRef]
60. Ehlers, T.A. Crustal Thermal Processes and the Interpretation of Thermochronometer Data. *Rev. Mineral. Geochem.* **2005**, *58*, 315–350. [CrossRef]
61. Liu, Y.S.; Gao, S.; Hu, Z.C.; Gao, C.G.; Zong, K.Q.; Wang, D.B. Continental and oceanic crust recycling-induced melt-peridotite interactions in the Trans-North China Orogen: U-Pb dating, Hf isotopes and trace elements in zircons from mantle xenoliths. *J. Petrol.* **2010**, *51*, 537–571. [CrossRef]
62. Windley, B.F.; Alexeiev, D.; Xiao, W.J.; Kroner, A.; Badarch, G. Tectonic models for accretion of the Central Asian Orogenic Belt. *J. Geol. Soc.* **2007**, *164*, 31–47. [CrossRef]
63. Xiao, W.J.; Windley, B.F.; Hao, J.; Zhai, M.G. Accretion leading to collision and the Permian Solonker suture, Inner Mongolia, China: Termination of the central Asian orogenic belt. *Tectonics* **2003**, *22*, 1069. [CrossRef]
64. Zhang, X.H.; Zhai, M.G. Magmatism and its metallogenetic effects during the Paleozoic continental crustal construction in northern North China: An overview. *Acta Petrol. Sin.* **2010**, *26*, 1329–1341. (In Chinese with English abstract)
65. Fan, G.H.; Li, J.W.; Deng, X.D.; Gao, W.S.; Li, S.Y. Age and origin of the Dongping Au-Te deposit in the North China Craton revisited: Evidence from paragenesis, geochemistry, and in situ U-Pb geochronology of garnet. *Econ. Geol.* **2021**, *116*, 963–985. [CrossRef]
66. Chang, E.Z.; Ying, X.D.; Zhou, A.; Wang, L.B. Geodynamic Evolution of Continental Margins in Eastern Asia and Tectonic Setting of East China Sea. In *Proceedings of the 29th International Geological Congress, Kyoto, Japan, 24 August–3 September, 1992*; Coleman, R.G., Ed.; Reconstruction of the Paleo-Asian Ocean; VSP: Rancho Cordova, CA, USA, 1994; pp. 133–167.
67. Tian, Z.Y.; Han, P.; Wu, K.D. The Mesozoic-Cenozoic East China rift system. *Tectonophysics* **1992**, *208*, 341–363. [CrossRef]
68. Fan, Q.C.; Liu, R.X. The high-temperature granulite xenoliths in Hannuoba basalt. *Chin. Sci. Bull.* **1996**, *117*, 251–284. (In Chinese)
69. Gao, S.; Luo, T.C.; Zhang, B.R.; Kern, H.; Zhao, Z.D. The chemical composition of the continental crust as revealed by studies in East China. *Geochim. Cosmochim. Acta* **1998**, *62*, 1959–1975. [CrossRef]
70. Li, C.J.; Bao, Z.W. Geochemical characteristics and geodynamic implications of the Early Cretaceous magmatisms in Zhangjiakou region, northwest Hebei Province, China. *Geochimica* **2012**, *41*, 343–358. (In Chinese with English abstract)
71. Qiu, X.P.; Hu, S.X.; Wang, J.; Wang, S. Gold mineralization of Xiaoyingpan quartz-carbonate type gold deposit, Hebei Province. *Acta Geol. Sin.* **1997**, *71*, 350–359. (In Chinese with English abstract)
72. Hu, X.D.; Chen, Z.H.; Zhao, Y.M.; Wang, K.Y. The metallogenetic epoch of the Xiaoyingpan gold deposit—The new material of U-Pb isotopic age on single zircon. *Prog. Precambrian Res.* **1997**, *20*, 22–28. (In Chinese with English abstract)

73. Wang, Z.K.; Jiang, X.M.; Wang, Y.; Shang, M.Y. A comparative analysis on geological and geochemical features of Xiaoyingpan and Dongping gold deposits, Hebei. *Geol. Prospect.* **1992**, *28*, 14–20. (In Chinese with English abstract)
74. Zhai, M.G.; Bian, A.G.; Zhao, T.P. The amalgamation of the supercontinent of North China Craton at the end of Neo-Archaean and its breakup during late Palaeoproterozoic and Meso-Proterozoic. *Sci. China Ser. D Earth Sci.* **2000**, *43*, 219–232. [CrossRef]
75. Zhai, M.G.; Zhao, L.; Zhu, X.Y.; Zhou, Y.Y.; Peng, P.; Guo, J.H.; Li, Q.L.; Zhao, T.P.; Lu, J.S.; Li, X.H. Late Neoarchean magmatic–metamorphic event and crustal stabilization in the North China Craton. *Am. J. Sci.* **2021**, *321*, 206–234. [CrossRef]
76. Wang, X.; Zhu, W.B.; Zheng, Y.F. Geochemical constraints on the nature of Late Archean basaltic-andesitic magmatism in the North China Craton. *Earth-Sci. Rev.* **2022**, *230*, 104065. [CrossRef]
77. Zhao, G.C.; Wilde, S.A.; Sun, M.; Guo, J.H.; Kröner, A.; Li, S.Z.; Li, X.P.; Zhang, J. SHRIMP U-Pb zircon geochronology of the Huai'an complex: Constraints on Late Archean to Paleoproterozoic magmatic and metamorphic events in the Trans-North China Orogen. *Am. J. Sci.* **2008**, *308*, 270–303. [CrossRef]
78. Liu, F.; Guo, J.H.; Lu, X.P.; Diwu, C.R. Crustal growth at ~2.5Ga in the North China Craton: Evidence from whole-rock Nd and zircon Hf isotopes in the Huai'an gneiss terrane. *Chin. Sci. Bull.* **2009**, *54*, 4704–4713.
79. Liu, S.W.; Lv, Y.J.; Wang, W.; Yang, P.T.; Bai, X.; Feng, Y.G. Petrogenesis of the Neoarchean granitoid gneisses in northern Hebei Province. *Acta Petrol. Sin.* **2011**, *27*, 909–921. (In Chinese with English abstract)
80. Zhai, M.G.; Guo, J.H.; Yan, Y.H.; Han, X.L.; Li, Y.G. The discovery of high-pressure basic granulite Terrain in North China Archaean Craton and preliminary study. *Sci. China Ser. B* **1993**, *36*, 1402–1408.
81. Guo, J.H.; Zhai, M.G.; Zhang, Y.G.; Li, Y.G.; Yan, Y.H.; Zhang, W.H. Early Precambrian Manjinggou high-pressure granulite mélange belt on the south edge of the Huai'an complex, North China craton: Geological features, petrology and isotopic geochronology. *Acta Petrol. Sin.* **1993**, *9*, 329–341. (In Chinese with English abstract)
82. Guo, J.H.; Sun, M.; Chen, F.K.; Zhai, M.G. Sm-Nd and SHRIMP U-Pb zircon geochronology of high-pressure granulites in the Sanggan area, North China Craton: Timing of Paleoproterozoic continental collision. *J. Asian Earth Sci.* **2005**, *24*, 629–642. [CrossRef]
83. Guo, L.; Wang, T.; Zhang, J.J.; Liu, J.; Qi, G.W.; Li, J.B. Evolution and time of formation of the Hohhot metamorphic core complex, North China: New structural and geochronological evidence. *Int. Geol. Rev.* **2012**, *54*, 1309–1331. [CrossRef]
84. Ren, J.Y.; Tamaki, K.; Li, S.T.; Zhang, J.X. Late Mesozoic and Cenozoic rifting and its dynamic setting in eastern China and adjacent areas. *Tectonophysics* **2002**, *344*, 175–205. [CrossRef]
85. Wang, T.; Guo, L.; Zheng, Y.; Donskaya, T.; Gladkochub, D.; Zeng, L.S.; Li, J.B.; Wang, Y.B.; Mazukabzov, A. Timing and processes of late Mesozoic mid-lower-crustal extension in continental NE Asia and implications for the tectonic setting of the destruction of the North China craton: Mainly constrained by zircon U-Pb ages from metamorphic core complexes. *Lithos* **2012**, *154*, 315–345. [CrossRef]
86. Li, J.W.; Vasconcelos, P.M.; Zhang, J.; Zhou, M.F.; Zhang, X.J.; Yang, F.H. $^{40}Ar/^{39}Ar$ constraints on a temporal link between gold mineralization, magmatism, and continental margin transtension in the Jiaodong gold province, eastern China. *J. Geol.* **2003**, *111*, 741–751. [CrossRef]
87. Tan, J.; Wei, J.H.; Audétat, A.; Pettke, T. Source of metals in the Guocheng gold deposit, Jiaodong Peninsula, North China craton: Link to early Cretaceous mafic magmatism originating from Paleoproterozoic metasomatized lithospheric mantle. *Ore Geol. Rev.* **2012**, *48*, 70–87. [CrossRef]
88. Zhu, R.X.; Fan, H.R.; Li, J.W.; Meng, Q.R.; Li, S.R.; Zeng, Q.D. Decratonic gold deposits. *Sci. China* **2015**, *58*, 1523–1537. [CrossRef]
89. Nie, F.J. Geology and origin of the Dongping alkalic-type gold deposit, northern Hebei province, People's Republic of China. *Resour. Geol.* **1998**, *48*, 139–158. [CrossRef]
90. Wang, Y.; Jiang, X.M.; Wang, Z.K. Characteristics of lead and sulfur isotope of the gold deposits in Zhangjiakou Xuanhua area Hebei Province. *Contrib. Geol. Mineral. Res.* **1990**, *2*, 66–75. (In Chinese with English abstract)
91. Zhang, H.; Yuan, H.L.; Hu, Z.C.; Liu, X.M.; Diwu, C.R. U-Pb zircon dating of the Mesozoic volcanic strata in Luanping of north Hebei and its significance. *Earth Sci.* **2005**, *30*, 707–720.